Systems/Circuits

Opposite Roles in Short-Term Plasticity for N-Type and P/Q-Type Voltage-Dependent Calcium Channels in GABAergic Neuronal Connections in the Rat Cerebral Cortex

Kiyofumi Yamamoto[1,2] and Masayuki Kobayashi[1,2,3]

[1]Department of Pharmacology, [2]Division of Oral and Craniomaxillofacial Research, Dental Research Center, Nihon University School of Dentistry, Chiyoda-ku, Tokyo 101-8310, Japan, and [3]Molecular Dynamics Imaging Unit, RIKEN Center for Life Science Technologies, Chuo-ku, Kobe 650-0047, Japan

Neurotransmitter release is triggered by Ca^{2+} influx through voltage-dependent Ca^{2+} channels (VDCCs). Distinct expression patterns of VDCC subtypes localized on the synaptic terminal affect intracellular Ca^{2+} dynamics induced by action potential-triggered Ca^{2+} influx. However, it has been unknown whether the expression pattern of VDCC subtypes depends on each axon terminal or neuronal subtype. Furthermore, little information is available on how these VDCC subtypes regulate the release probability of neurotransmitters. To address these questions, we performed multiple whole-cell patch-clamp recordings from GABAergic neurons in the insular cortex of either the male or the female rat. The paired-pulse ratio (PPR; 50 ms interstimulus interval) varied widely among inhibitory connections between GABAergic neurons. The PPR of unitary IPSCs was enhanced by ω-conotoxin GVIA (CgTx; 3 μM), an N-type VDCC blocker, whereas blockade of P/Q-type VDCCs by ω-agatoxin IVA (AgTx, 200 nM) decreased the PPR. In the presence of CgTx, application of 4 mM $[Ca^{2+}]_o$ or of roscovitine, a P/Q-type activator, increased the PPR. These results suggest that the recruitment of P/Q-type VDCCs increases the PPR, whereas N-type VDCCs suppress the PPR. Furthermore, we found that charybdotoxin or apamin, blockers of Ca^{2+}-dependent K^+ channels, with AgTx increased the PPR, suggesting that Ca^{2+}-dependent K^+ channels are coupled to N-type VDCCs and suppress the PPR in GABAergic neuronal terminals. Variance–mean analysis with changing $[Ca^{2+}]_o$ showed a negative correlation between the PPR and release probability in GABAergic synapses. These results suggest that GABAergic neurons differentially express N-type and/or P/Q-type VDCCs and that these VDCCs regulate the GABA release probability in distinct manners.

Key words: agranular; AI; calcium channel; parvalbumin; STP; VGCC

Significance Statement

GABAergic neuronal axons target multiple neurons and release GABA triggered by Ca^{2+} influx via voltage-dependent Ca^{2+} channels (VDCCs), including N-type and P/Q-type channels. Little is known about VDCC expression patterns in GABAergic synaptic terminals and their role in short-term plasticity. We focused on inhibitory synaptic connections between GABAergic neurons in the cerebral cortex using multiple whole-cell patch-clamp recordings and found different expression patterns of VDCCs in the synaptic terminals branched from a single presynaptic neuron. Furthermore, we observed facilitative and depressive short-term plasticity of IPSCs mediated by P/Q-type and N-type VDCCs, respectively. These results suggest that VDCC expression patterns regulate distinctive types of synaptic transmission in each GABAergic axon terminal even though they are branched from a common presynaptic neuron.

Introduction

Short-term plasticity depends on neuronal activities and is ubiquitously observed in both excitatory and inhibitory synapses in the CNS (Atluri and Regehr, 1996; Reyes et al., 1998; Neher and Sakaba, 2008; Yamamoto et al., 2010a; Satake and Imoto, 2014).

Received Feb. 6, 2018; revised July 23, 2018; accepted July 28, 2018.

Author contributions: K.Y. and M.K. designed research; K.Y. performed research; K.Y. and M.K. analyzed data; K.Y. and M.K. wrote the paper.

This work was supported by KAKENHI Grants 25861764 and 17K11653 to K.Y. and Grants 16K15873 and 16H05507 to M.K. from the The Ministry of Education, Culture, Sports, Science and Technology (MEXT); by grants from the Sato and Uemura Foundations; and by the MEXT-Supported Program for Strategic Research Foundation at Private Universities, 2013–2017, to M.K. VGAT-Venus transgenic rats were generated by Drs. Y. Yanagawa, M. Hirabayashi, and Y. Kawaguchi at the National Institute for Physiological Sciences (Okazaki, Japan), using pCS2-Venus provided by Dr. A. Miyawaki. We thank Prof. S. Mochida for advice on the discussion. We thank Prof. N. Koshikawa for critical reading of this manuscript.

Correspondence should be addressed to Dr. Masayuki Kobayashi, Department of Pharmacology, Nihon University School of Dentistry, 1-8-13 Kanda-Surugadai, Chiyoda-ku, Tokyo 101-8310, Japan. E-mail: kobayashi.masayuki@nihon-u.ac.jp.

https://doi.org/10.1523/JNEUROSCI.0337-18.2018

 0270-6474/18/389814-15$15.00/0

The interval of repetitive spike firing delivered to the presynaptic terminal affects the kinetics of consecutive transmitter releases, i.e., facilitation or depression. Several mechanisms have been postulated to explain short-term plasticity (Blitz et al., 2004). In terms of paired-pulse depression, an initial high probability of transmitter release leads to depletion of synaptic vesicles released in response to the second action potential. On the other hand, a number of mechanisms have been proposed to account for paired-pulse facilitation (Xu-Friedman and Regehr, 2004). Zucker and Regehr (2002) demonstrated that residual Ca^{2+} in the synaptic terminal with a low initial probability of release accumulates during repeated stimulation at a short interstimulus interval, resulting in a transient increase in release probability and inducing a facilitative synaptic response.

Several types of voltage-dependent Ca^{2+} channels (VDCCs), P/Q type (CaV 2.1) and N type (CaV 2.2), serve a critical role in the process of fast vesicle fusion and transmitter release both in excitatory and inhibitory synaptic terminals (Dunlap et al., 1995; Ishikawa et al., 2005). Previous reports focusing on neurotransmitter release in invertebrate and vertebrate synapses demonstrate that properties of transmitter release are strongly influenced by Ca^{2+} dynamics in the synaptic terminal (Augustine et al., 1985; Schneggenburger and Neher, 2005). Iwasaki and Takahashi (2001) reported not only an age-dependent switching of VDCC subtypes but also a decrease in paired-pulse depression that occurs in the calyx of Held during the early postnatal stage. Interestingly, in hippocampal CA1 synapses, two connections, i.e., a common presynaptic pyramidal cell targeting both another postsynaptic pyramidal and GABAergic neurons, demonstrate different profiles of short-term plasticity, indicating that a mechanism for a divergent synaptic efficacy is inherent in each terminal branched from a common presynaptic neuron. Although electromicroscopic studies have demonstrated the coexistence of P/Q-type and N-type VDCCs in mature synaptic terminals (Éltes et al., 2017), electrophysiological studies propose that each terminal expresses either P/Q-type or N-type VDCCs, which determines the manner of transmitter release (Horne and Kemp, 1991; Zaitsev et al., 2007). Therefore, it remains controversial which VDCC subtype is expressed in each terminal and how these VDCCs regulate short-term plasticity (Toledo-Rodriguez et al., 2004; Ali and Nelson, 2006; Zaitsev et al., 2007).

GABAergic neurons in the cerebral cortex and hippocampus form inhibitory synapses not only to excitatory pyramidal neurons but also to various GABAergic neuronal subtypes (Letzkus et al., 2015; Tremblay et al., 2016). The connections among GABAergic interneurons attenuate the inhibition of excitatory neurons by inhibiting presynaptic GABAergic neurons in a process called disinhibition (Kisvárday et al., 1993; Pfeffer et al., 2013; Tremblay et al., 2016). Recent behavioral studies using optogenetic techniques demonstrate that the microcircuit of disinhibition regulates several behavioral functions, such as sensorimotor integration, social behavior attention, and auditory fear conditioning (Letzkus et al., 2015). Cortical fast-spiking neurons (FSNs) connect not only to pyramidal cells but also to FSNs and other types of GABAergic interneurons (non-FSNs) with a high connection rate and impact (Pfeffer et al., 2013), and FSNs are therefore considered to play a critical role in the regulation of cortical functions. Clarification of the VDCC composition in GABAergic synapses among GABAergic neurons and the profile of short-term plasticity elucidate the mechanisms underlying disinhibition-mediated functions of the cerebral cortex.

We performed multiple whole-cell patch-clamp recordings and analyzed unitary inhibitory postsynaptic currents (uIPSCs) to investigate the short-term plasticity profile between presynaptic FSNs and postsynaptic GABAergic interneurons. Our results demonstrated that (1) VDCC subtypes, i.e., P/Q-type and N-type VDCCs, are not homogenously expressed in each axon terminal even if they branch from the same presynaptic FSN, and (2) P/Q-type and N-type VDCCs increased and decreased, respectively, the paired-pulse ratios (PPRs) in connections between FSNs and either FSNs or non-FSNs.

Materials and Methods

All experiments were performed in accordance with the National Institutes of Health *Guide for the Care and Use of Laboratory Animals* and were approved by the Institutional Animal Care and Use Committee at Nihon University. All efforts were made to minimize the number of animals used and their suffering.

Slice preparations. The data reported below consist of results from 137 vesicular GABA transporter (VGAT)-Venus line A transgenic rats (Nagai et al., 2002; Uematsu et al., 2008). The techniques for preparing *in vitro* cortical slices were similar to those described previously (Takei et al., 2017). Briefly, rats of either sex, ages 17–32 d, were deeply anesthetized with isoflurane (5%). After decapitation, tissue blocks including the insular cortex (IC) were rapidly removed and stored for 3 min in ice-cold modified artificial CSF (ACSF) containing the following (in mM): 230 sucrose, 2.5 KCl, 10 $MgSO_4$, 1.25 NaH_2PO_4, 26 $NaHCO_3$, 0.5 $CaCl_2$, and 10 D-glucose. Coronal slices were cut at a thickness of 350 μm using a microslicer (Linearslicer Pro 7, Dosaka EM). Slices were incubated at 32°C for 15 min in a submersion-type holding chamber that contained 50% modified ACSF and 50% normal ACSF, pH 7.35–7.40. Normal ACSF contained (in mM) 126 NaCl, 3 KCl, 2 $MgSO_4$, 1.25 NaH_2PO_4, 26 $NaHCO_3$, 2 $CaCl_2$, and 10 D-glucose. Modified and normal ACSF were continuously aerated with a mixture of 95% O_2/5% CO_2. The slices were transferred to a holding chamber with normal ACSF at 32°C for 1 h and thereafter maintained at room temperature until used for recording.

Multiple whole-cell patch-clamp recordings. The slices were placed in a recording chamber that was perfused continuously with normal ACSF at a rate of 2.0 ml/min. To minimize the adherence of peptidergic drugs to the perfusion route, we used the infusion pump whose head was made of polytetrafluoroethylene (Q-100-TT-P-S, Tacmina) and silicon tubes (C-flex tubing, Cole-Parmer Instrument). Multiple whole-cell patch-clamp recordings were obtained from Venus-positive fluorescent GABAergic interneurons identified in layer V by using a fluorescence microscope equipped with Nomarski optics (40×, Olympus BX61W1) and an infrared-sensitive video camera (C3077-78, Hamamatsu Photonics). The distance between recorded cells was <75 μm. Electrical signals were recorded with amplifiers (Multiclamp 700B, Molecular Devices) and a digitizer (Digidata 1440A, Molecular Devices), observed on-line, and stored on a computer hard disk using Clampex (pClamp 10, Molecular Devices).

The composition of the pipette solution was as follows (in mM): 85 potassium gluconate, 70 KCl, 10 HEPES, 0.5 EGTA, 2 $MgCl_2$, 2 magnesium ATP, and 0.3 sodium GTP. The pipette solution had a pH of 7.3 and an osmolarity of 300 mOsm. The equilibrium potential of Cl^- (E_{Cl^-}) was −15 mV. In the experiment measuring the kinetics of action potentials, the pipette solution contained the following (E_{Cl} = −65 mV; in mM): 135 potassium gluconate, 10 HEPES, 0.5 EGTA, 2 $MgCl_2$, 2 magnesium ATP, and 0.3 sodium GTP. The liquid junction potentials of the high- and low-$[Cl^-]_i$ pipette solutions described above were −9 and −6 mV, respectively. The voltage was not corrected in the present study. Thin-wall borosilicate patch electrodes (2–5 MΩ) were pulled on a Flaming-Brown micropipette puller (P-97, Sutter Instruments). Alexa Fluor 594 (Invitrogen) was added to the internal solution in a subset of the experiments (Fig. 1*A*).

Recordings were obtained at 30−31°C. The seal resistance was >10 GΩ, and only data obtained from electrodes with an access resistance of 6–20 MΩ and <20% change during recordings were included in this study. Before uIPSC recordings, the voltage responses of presynaptic and postsynaptic GABAergic cells were recorded by injection of depolarizing and hyperpolarizing current pulses (300 ms) to examine basic membrane properties, including input resistance, single-spike kinetics, voltage–cur-

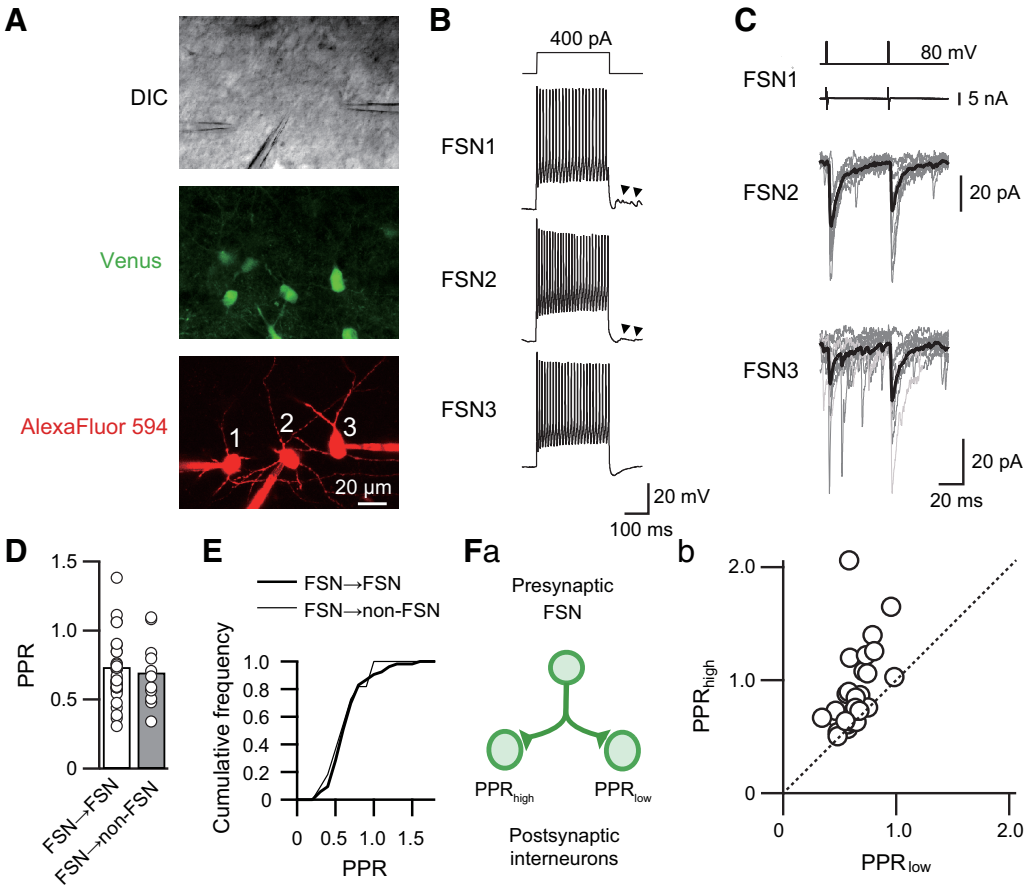

Figure 1. Divergent PPRs obtained from two GABAergic connections composed of a common presynaptic FSN targeting different postsynaptic GABAergic neurons. ***A***, Triple whole-cell patch-clamp recordings were performed in layer V of the insular cortex under differential interference contrast infrared video microscopy (DIC). Green and red fluorescent images indicate VGAT-Venus-positive neurons (Venus) and Alexa Fluor 594 added into the internal solution for visualization of somatic and dendritic shapes of recorded neurons, respectively. ***B***, Firing properties of three Venus-positive neurons (FSN1–3) induced by depolarizing current pulse injections (300 ms) to the neurons shown in ***A***. These neurons were classified as FSNs based on a large and fast afterhyperpolarization and high-frequency spike firing without spike adaptation. Synaptic inputs via autapses were observed after the end of repetitive spike firing (arrowheads). These responses were depolarized because the internal solution contains a high concentration of Cl^-. ***C***, Distinct short-term plasticity observed in FSN1⟶FSN2 and FSN1⟶FSN3 connections. Postsynaptic uIPSCs recorded from FSN2 and FSN3 were induced by paired depolarizing voltage pulses to FSN1 (top traces) that induced action currents (the second traces from the top). FSN1⟶FSN2 and FSN1⟶FSN3 connections showed PPRs of 0.80 and 1.37, respectively. Gray and black lines indicate 11 consecutive traces and their averaged traces, respectively. ***D***, Mean PPRs in FSN⟶FSN ($n = 53$) and FSN⟶non-FSN ($n = 11$) connections. There were no significant differences in PPRs between these connections. ***E***, Cumulative curves of PPRs obtained from FSN⟶FSN and FSN⟶non-FSN connections. There were no significant differences between these curves. ***Fa***, Relationship between PPRs obtained from two connections with a common presynaptic FSN. ***Fb***, Larger and smaller PPRs were plotted onto the abscissa and ordinate, respectively. The data were obtained from 26 pairs of connections. Note that most plots are not on the dotted identity line.

rent relationship, and repetitive firing patterns and frequency. Because some cell pairs had reciprocal or two or more connections, most cells were recorded under voltage-clamp conditions (holding potential, −60 mV) during uIPSC recording. Short depolarizing voltage step pulses (2 ms, 80–120 mV) were applied to the presynaptic cells to induce action currents at 15 s interval. In the experiments using Ca^{2+}-dependent K^+ (K_{Ca}) channel blockers, presynaptic cells were stimulated by short depolarizing current pulses (0.5 ms) to evoke action potentials under a current-clamp condition to examine the blockers' effect on presynaptic action potentials. The membrane currents and potentials were low-pass filtered at 5–10 kHz and digitized at 20 kHz.

VDCC blockers, ω-conotoxin GVIA (CgTx; 3 μM; Peptide Institute) and ω-agatoxin IVA (AgTx; 200 nM; Peptide Institute) were added directly to the perfusate. For the variance–mean analysis, we measured uIPSC amplitude under the application of ACSF with different $[Ca^{2+}]_o$ (0.5, 1.0, 2.0, and 4.0 mM). $[Mg^{2+}]_o$ was kept constant (2.0 mM) when $[Ca^{2+}]_o$ was ≤2.0 mM and kept at 1.0 mM in the recording under 4.0 mM $[Ca^{2+}]_o$ (Yamamoto et al., 2010b; Almado et al., 2012). A stock solution of (*R*)-2-(1-ethyl-2-hydroxyethylamino)-6-benzylamino-9-isopropylpurine (roscovitine, 30 μM; Cell Signaling Technology) was prepared in dimethylsulfoxide at 50 mM. Apamin (1 μM, Peptide Institute) and charybdotoxin (ChTx; 50–100 nM, Peptide Institute) were also added to the perfusate. Bicuculline (10 μM, Sigma-Aldrich) was added to block the $GABA_A$ receptor-mediated component. uIPSC amplitude during drug application was recorded and monitored on-line. To obtain the steady uIPSC amplitude, drugs were applied for at least 10 min. We excluded the recordings that showed a significant correlation between uIPSC amplitude and time (150 s) as we previously described (Koyanagi et al., 2010). After reaching the steady state, the next drug was applied. Other compounds were purchased from Wako Pure Chemical Industries or Nakalai Tesque.

Experimental design and statistical analysis. Clampfit (pClamp 10, Molecular Devices) was used for analysis of electrophysiological data. The averaged amplitude and PPR determined by the ratio of the peak amplitude of the second uIPSCs to that of the first uIPSCs were obtained from 10–20 consecutive sweeps. The failure of uIPSCs was defined to be less than three times the SD of the base line. PPRs were excluded from the analysis if uIPSC responses showed a 50% failure rate during the application of AgTx.

The variance–mean analysis was performed as described previously (Silver, 2003; Yamamoto et al., 2010b; Almado et al., 2012). Briefly, we obtained 20–40 uIPSC responses in each $[Ca^{2+}]_o$, and the mean uIPSC amplitude (M) was calculated and plotted against their variance (V). Individual plots were fitted with a quadratic equation assuming zero

variance at zero amplitude. The quantal content (q) and number of release sites (N) were estimated by using the following equation: $V = qM - M^2/N$.

The release probability (Pr) was estimated by the following equation: $Pr = M/qN$, where M is divided by the averaged uIPSC amplitude in 2 mM $[Ca^{2+}]_o$. In this study, intrasite and intersite quantal variances described by Silver (2003) were not estimated, and thus it is presumed that putative individual release sites exhibit equal variances.

The values are expressed as the mean ± SEM. Differences in the mean values between two groups were compared with the paired t test or Student's t test. One-way ANOVA was used to compare spike kinetics among three groups. The paired t test with Bonferroni's correction was used in the case of two comparisons among three groups. The Kolmogorov–Smirnov test was used for a comparison of distributions. Correlations between variables were evaluated with the parametric Pearson and nonparametric Spearman correlation tests. Differences with $p < 0.05$ were considered significant.

Results

The present study focused on GABAergic synaptic transmission between GABAergic interneurons in layer V of IC. To discriminate glutamatergic from GABAergic neurons, we used VGAT-Venus line A transgenic rats in which GABAergic neurons are marked with a green fluorescent protein, Venus.

Different short-term plasticity at synapses from a common presynaptic FSN

GABAergic neurons in IC are classified as FSNs or non-FSNs based on their membrane properties, including spike kinetics and repetitive firing properties and duration. FSNs are characterized by a high firing rate (typically >100 Hz) without spike adaptation, short spike duration, and large and short afterhyperpolarization (Kawaguchi and Kubota, 1997; Galarreta and Hestrin, 2002; Koyanagi et al., 2010, 2014; Fig. 1*B*). Autaptic responses, which were blocked by bicuculline (10 μM; data not shown), were often observed just after the end of the depolarizing pulse applied to FSNs (Fig. 1*B*, arrowheads). In the present study, we quantitatively identified Venus-positive neurons as FSNs that showed <1.25 of the adaptation ratio (last interspike interval/first interspike interval; Kröner et al., 2007). On the other hand, non-FSNs include neurons showing low-threshold spiking, late spiking, and regular spiking (Koyanagi et al., 2010; Yamamoto et al., 2010a).

Alexa Fluor 594 present in the internal patch solution was used to visualize three different Venus-positive neurons (Fig. 1*A*) that showed repetitive spike firing classified as FSNs (Fig. 1*B*). The presynaptic FSN1 induced different kinetics of short-term plasticity in the postsynaptic FSN2 and FSN3 (Fig. 1*C*): the FSN1 projection to postsynaptic FSN2 exhibited paired-pulse depression (PPR, 0.80), whereas the FSN1→FSN3 connection showed paired-pulse facilitation (PPR, 1.37). Application of 10 μM bicuculline, a $GABA_A$ receptor antagonist, completely blocked uIPSCs (data not shown). This finding suggests that even the same postsynaptic GABAergic neuronal subtype and a common presynaptic FSN could induce different kinetics of short-term plasticity.

This variation in the PPR was independent of postsynaptic neuronal subtypes. We compared PPRs in the control between FSN→FSN and FSN→non-FSN connections. The mean PPR of FSN→FSN connections (0.73 ± 0.03, $n = 53$) was comparable with that of FSN→non-FSN connections (0.70 ± 0.07, $n = 11$; $t_{(62)} = 0.481$, $p = 0.63$, Student's t test; Fig. 1*D*), and the cumulative plots of these connections were also comparable ($p = 0.99$, Kolmogorov–Smirnov test; Fig. 1*E*). Furthermore, comparison of the PPR between postsynaptic non-FSNs, late-spiking neurons ($n = 7$), and regular spiking neurons ($n = 4$), showed an insignificant difference ($t_{(9)} = 0.407$, $p = 0.694$, Student's t test). These results suggest that the PPR is independent of postsynaptic GABAergic neuronal subtypes.

The summarized result of triple whole-cell patch-clamp recordings that consisted of a common presynaptic FSN and two postsynaptic FSNs/non-FSNs is shown in Figure 1*F*. Although several points are located close to the identity line, which indicates the same PPR in two connections, most dots were sparsely distributed. This result indicates that subsets of paired connections showed distinct PPRs in each synapse despite a common presynaptic FSN. Thus, it is likely that each GABA release site has different properties of short-term plasticity.

N-type and P/Q-type VDCC blockers suppress uIPSCs in FSN→FSN/non-FSN connections

uIPSCs were suppressed by bath application of VDCC blockers. Among these blockers, the selective N-type VDCC blocker CgTx and the selective P/Q-type VDCC blocker AgTx were the most effective in suppressing uIPSCs, as shown in Figure 2. An example of the effects of CgTx (3 μM) and AgTx (200 nM) showed that the application of these two VDCC blockers almost completely abolished uIPSCs and that the residual component of uIPSCs was negligible (Fig. 2*A*,*B*). The effectiveness of CgTx and AgTx differed between FSN1→FSN2 and FSN3→non-FSN connections: FSN1→FSN2 connections were less sensitive to CgTx than FSN3→non-FSN connections, although AgTx almost completely abolished uIPSCs in both connections.

In summary, there was no significant difference in the rate of suppression of uIPSC amplitude induced by CgTx and AgTx between FSN→FSN and FSN→non-FSN connections (CgTx: FSN, 15.8 ± 2.4%, $n = 53$; non-FSN, 18.2 ± 5.4%, $n = 11$, $t_{(62)} = 0.417$, $p = 0.791$; AgTx: FSN, 69.7 ± 3.0%, $n = 53$; non-FSN, 68.0 ± 6.0%, $n = 11$, $t_{(62)} = 0.239$, $p = 0.812$, Student's t test; Fig. 2*C*). Considering the comparable PPRs (Fig. 1*D*,*E*) with similar sensitivities to CgTx and AgTx between FSN→FSN and FSN→non-FSN connections (Fig. 2*C*), the subsequent statistical analyses were performed using combined data obtained from FSN→FSN and FSN→non-FSN connections.

PPR of uIPSCs depends on sensitivity to VDCCs

Recent studies of cultured superior cervical ganglion (SCG) neurons that artificially express either P/Q- or N-type VDCCs demonstrate that the differential expression of these VDCC subtypes provides distinct short-term plasticity (Mochida et al., 2008; Mori et al., 2014). Moreover, in several excitatory synapses, including calyx of Held and hippocampal and cultured SCG synapses, Ca^{2+} influx via P/Q-type VDCCs induces paired-pulse facilitation (Iwasaki and Takahashi, 2001; Brown and Randall, 2005; Mochida et al., 2008; Nanou et al., 2016). To investigate whether the involvement of P/Q-type VDCCs increases the PPR of uIPSCs, we examined the effects of CgTx (3 μM) and AgTx (200 nM) on PPRs obtained from GABAergic connections between a common presynaptic FSN and postsynaptic FSNs/non-FSNs (Fig. 3).

Figure 3*A*–*C* shows an example of the effects of CgTx and AgTx on uIPSC amplitude and PPR in FSN→non-FSN connections. The synaptic responses in the FSN→non-FSN1 connection showed slight paired-pulse depression (PPR, 0.63; Fig. 3*B*). On the other hand, the FSN→non-FSN2 connection, which included the same presynaptic FSN as in the FSN→non-FSN1 connection, showed potent paired-pulse depression (PPR, 0.34; Fig. 3*B*). Bath application of CgTx had little effect on uIPSC amplitude and PPR (0.69) in the FSN→non-FSN1 connection, whereas the FSN→non-FSN2 connection showed a shift from

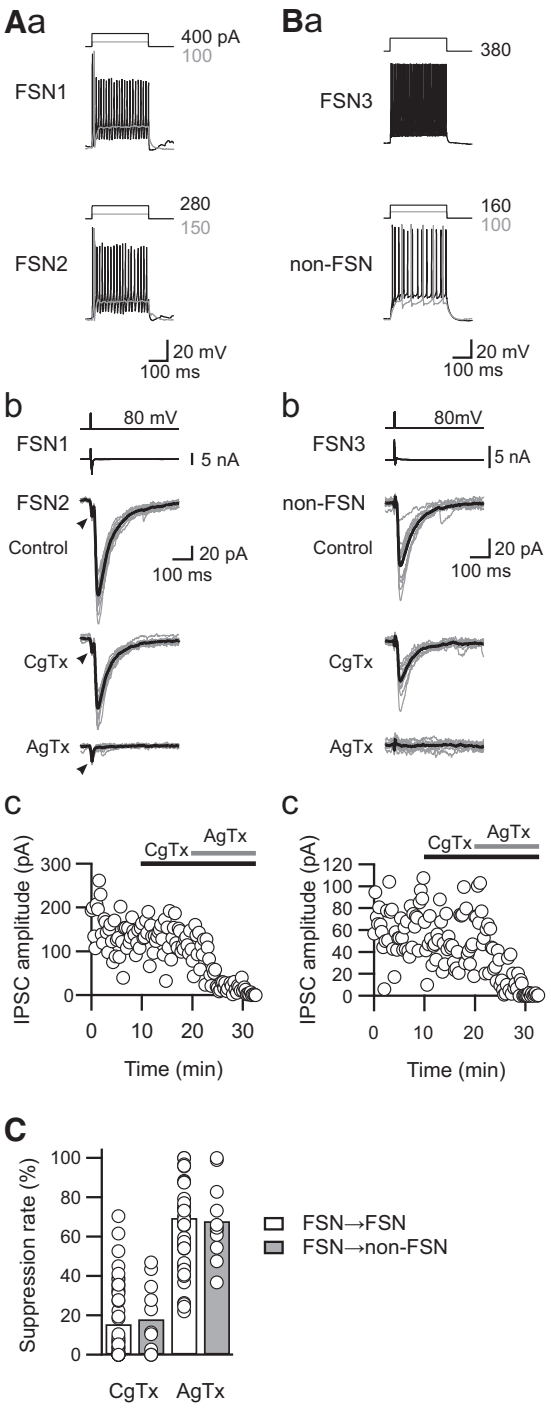

Figure 2. Sensitivity of uIPSCs to N- and P/Q-type VDCC blockers. ***A***, ***B***, Effects of CgTx (3 μM) and AgTx (200 nM) on uIPSCs obtained from the FSN1→FSN2 connection (***A***) and from the FSN→non-FSN connection (***B***). Firing properties of presynaptic FSNs and postsynaptic FSN/non-FSN in response to depolarizing current pulse injection are shown in ***Aa*** and ***Ba***. Note that CgTx partially suppressed uIPSCs in both connections, and AgTx completely blocked the residual uIPSCs (***Ab***, ***Bb***). Top traces represent voltage-step pulses for induction of action currents in presynaptic FSNs (the second traces from the top). Arrowheads indicate the response mediated by gap junction. Time courses of uIPSC amplitude are shown in ***Ac*** and ***Bc***. ***C***, Summary of sensitivities of uIPSCs to VDCC blockers in FSN→FSN ($n = 53$) and FSN→non-FSN ($n = 11$) connections. No significant differences were observed between these connections.

paired-pulse depression to facilitation (PPR, 1.09) with a decrease in the first uIPSC amplitude. Sequential application of AgTx almost abolished uIPSCs in both connections, and PPRs of the FSN→non-FSN1 and non-FSN2 connections were too small in amplitude to be estimated. These results suggest the distinct expression of N-type and P/Q-type VDCCs in each connection that receives inputs from the same presynaptic FSN. Moreover, it is likely that N-type and P/Q-type VDCCs play reciprocal roles in the regulation of PPRs: suppressive and facilitative effects, respectively, on PPRs.

To confirm this possibility, we compared PPRs under either AgTx or CgTx application with that in the control. A typical example of the effect of AgTx is shown in Figure 3*C*. Bath application of AgTx decreased the amplitude of both the first and second uIPSCs (Fig. 3*Cb*). In parallel to the decrease in uIPSC amplitude, AgTx also changed the profile of short-term plasticity: AgTx decreased the PPR from 0.71 to 0.58 (Fig. 3*Cc*). Summary results showed a decrease in the PPR by AgTx (0.69 ± 0.04 in control and 0.53 ± 0.05 under AgTx application, $n = 16$. $t_{(15)} = 2.773$, $p = 0.014$, paired t test; Fig. 3*Da*) and an increase in the PPR with CgTx (0.67 ± 0.03 in control and 0.78 ± 0.06 under CgTx application, $n = 22$, $t_{(21)} = 2.143$, $p = 0.044$, paired t test; Fig. 3*Db*). These summarized results support the hypothesis described above.

We analyzed dual, triple, and quadruple recordings that involved one, two, and three FS→FSN/non-FSN connections, respectively, to explore the relationship between AgTx-sensitive percentages of uIPSCs and PPR in the control condition. There was a positive correlation between the PPR in the control and the effect on AgTx on the first uIPSC amplitude ($n = 65$, $\rho = 0.479$, $p = 0.0001$, Spearman correlation; Fig. 3*E*): the connections with larger PPRs in the control showed higher sensitivity to AgTx. This relationship suggests that AgTx-sensitive components of uIPSCs contribute to the induction of high PPRs.

The diversity of PPRs in each connection suggests the distinct expression pattern of VDCCs. To examine this possibility, the effects of N-type and P/Q-type VDCC blockers were tested in triple whole-cell patch-clamp recordings, and the sensitivity of each VDCC blocker to IPSC amplitude was compared between the connections that received common inhibitory inputs from the same presynaptic FSNs. Bath application of 3 μM CgTx showed an imbalance in the suppression rate of uIPSC amplitude (Fig. 3*Fa*): six pairs of connections showed comparable suppression rates, whereas the other five pairs showed a large difference in the suppression rate between the pair connections. The inconsistent suppression rate of uIPSC amplitude by CgTx was also observed in the case of AgTx (200 nM) application (Fig. 3*Fb*). These results suggest that expression patterns of N-type and P/Q-type VDCCs are not consistent even in the connections branched from the same presynaptic FSN.

$[Ca^{2+}]_o$ changes release probability of GABA

It has been demonstrated that the PPR closely correlates with the release probability of neurotransmitters. A higher release probability induces a larger amount of neurotransmitter release and decreases the amount of neurotransmitter in the readily releasable pool. Thus, in the case that a presynaptic terminal induces action potentials at a short interspike interval, the second release of neurotransmitter is diminished, and as a result, the PPR is decreased (Yamamoto et al., 2010b; Counotte et al., 2011). However, several studies report no correlation between release probability and PPR in glutamatergic synapses (Bellingham and Walmsley, 1999; Yang and Xu-Friedman, 2008) and in $GABA_A$ receptor-mediated synapses (Overstreet et al., 2000), one of whose mechanisms is postulated to be desensitization of postsynaptic receptors. Other previous studies demonstrate that lowering the $[Ca^{2+}]_o$ in ACSF decreases the amplitude of the first

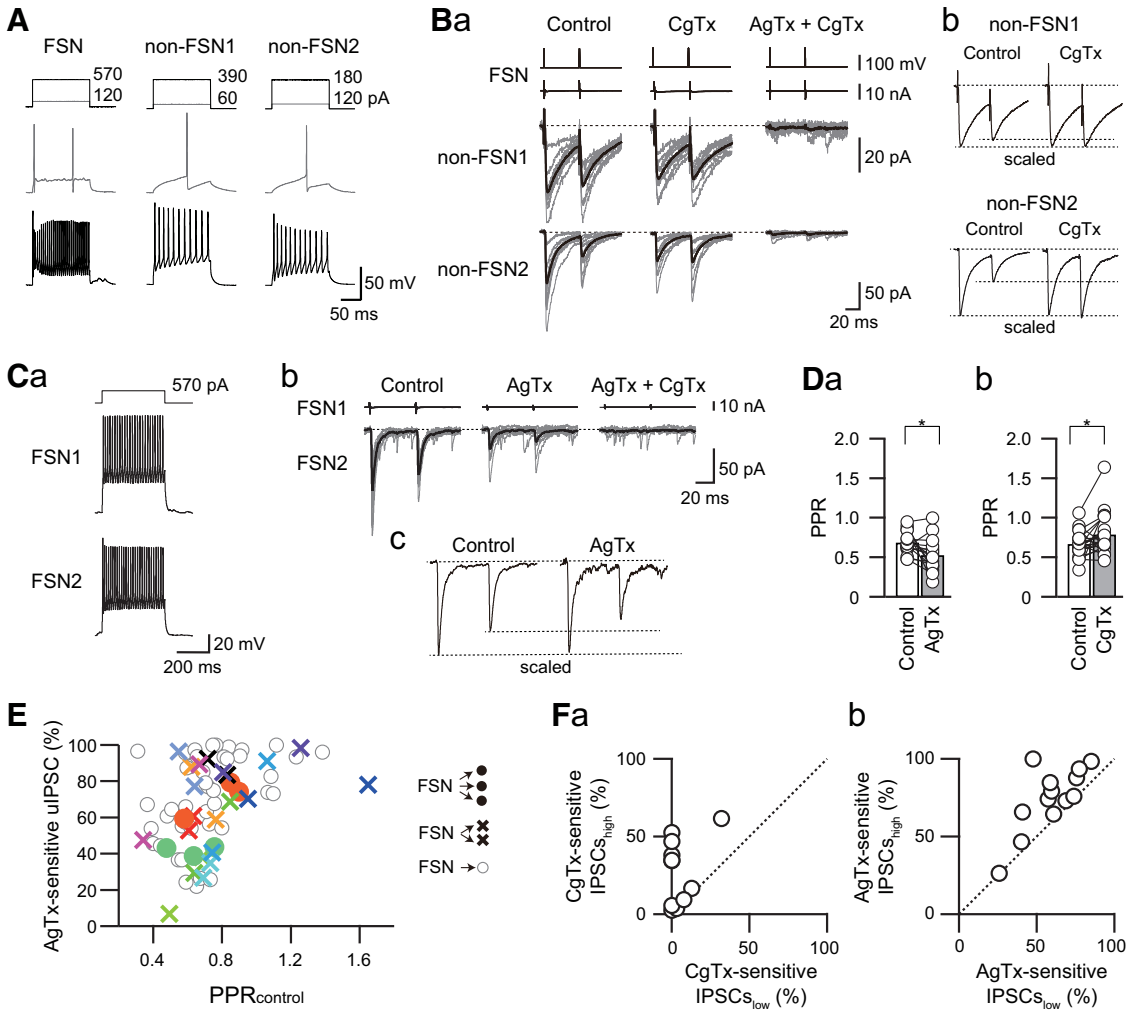

Figure 3. Different sensitivities of uIPSCs to P/Q- and N-type VDCC blockers in connections sharing a presynaptic FSN. ***A***, Firing properties of presynaptic FSNs and two different postsynaptic non-FSNs in response to depolarizing current pulse injection. ***B***, Effects of CgTx (3 μM) on IPSC amplitudes in the FSN→non-FS connections. ***Ba***, Note that these connections exhibited different sensitivities of uIPSCs to CgTx. ***Bb***, Scaled traces clearly showed that CgTx increased the PPR in the FSN→non-FSN2 connection. ***C***, The effects of AgTx (200 nM) on the PPR in the FSN1→FNS2 connection. ***Ca***, Repetitive spike firing of presynaptic and postsynaptic FSNs (FSN1 and FSN2, respectively). ***Cb***, Effects of AgTx on uIPSCs in the FSN1→FSN2 connection. ***Cc***, Scaled traces in the control and the N-type VDCC-mediated components isolated by AgTx showed the suppression of PPR. ***D***, Summary of the effects of AgTx (***a***) and CgTx (***b***) on FSN→FSN/non-FSN connections. Note the significant suppression and facilitation of the PPR by AgTx ($n = 16$) and by CgTx ($n = 22$), respectively (*$p < 0.05$, paired t test). ***E***, Relationship between the PPR obtained from control ($PPR_{control}$, abscissa) and the percentage of AgTx-sensitive uIPSCs (ordinate) recorded from one (open circles), two (crosses), and three (closed circles) connections consisting of common presynaptic FSNs. The plots with the same colors represent paired connections with a common presynaptic FSN. Note a positive correlation between $PPR_{control}$ and the percentage of AgTx-sensitive uIPSCs ($\rho = 0.479$, $p < 0.0001$, $n = 65$, Spearman correlation). ***F***, Relationship of CgTx sensitivities (***a***) and AgTx sensitivities (***b***) between two postsynaptic neurons receiving synaptic inputs from a common FSN. The sensitivities to CgTx (***a***) and AgTx (***b***) with high and low values are plotted onto the abscissa and ordinate, respectively (CgTx, $n = 11$; AgTx, $n = 13$). Note the sparse distribution of plots.

EPSCs and increases the PPR by suppressing neurotransmitter release in excitatory synapses (Oleskevich et al., 2000). Therefore, we performed variance–mean analysis by changing the $[Ca^{2+}]_o$ from 0.5 to 4.0 mM, which changes release probability (Silver et al., 1998), to examine the relationship between release probability and PPR in GABAergic synapses.

A typical example of the effect of $[Ca^{2+}]_o$ on uIPSC amplitude obtained from an FSN→FSN connection showed that the higher $[Ca^{2+}]_o$ induced a larger uIPSC amplitude (Fig. 4*Ba*). Figure 4*Bb* shows paired-pulse responses whose first uIPSC amplitude is scaled. Higher $[Ca^{2+}]_o$ induced larger uIPSCs and a lower PPR. The consecutive first uIPSC amplitude recorded under the application of different $[Ca^{2+}]_o$ is shown in Figure 4*C*. The variance in each $[Ca^{2+}]_o$ was plotted against the mean amplitude of uIPSC to obtain the parabolic function that fits to the plots (Fig. 4*D*). We estimated the release probability, the number of release sites, and quantal content by using variance–mean analysis (Fig. 4*E*).

There was a significant correlation between release probability and PPR ($n = 14$, $r = -0.545$, $p = 0.044$, Pearson correlation; Fig. 4*Ea*). However, little correlation was observed between quantal size and PPR ($n = 14$, $r = -0.459$, $p = 0.099$, Pearson correlation; Fig. 4*Eb*) and between the number of release sites and PPR ($n = 14$, $r = 0.091$, $p = 0.758$, Pearson correlation; Fig. 4*Ec*). These results indicate that the PPR reflects release probability in IC GABAergic synapses.

Enhancement of PPR by increasing $[Ca^{2+}]_o$ in combination with an N-type VDCC blocker

In terms of the CgTx-induced increase in PPR, several possible mechanisms could be hypothesized. First, a facilitative effect of CgTx on the PPR could be attributed to a decrease in release probability merely by decreasing Ca^{2+} influx via N-type VDCCs. It is also possible to presume that Ca^{2+} influx via P/Q-type VDCCs increases PPR. To examine these possibilities, we elucidated

the effect of high $[Ca^{2+}]_o$ under the application of CgTx on PPR: if P/Q-type VDCCs contribute to an increase in PPR, an increase in Ca^{2+} influx via P/Q-type VDCCs by replacing the normal ACSF with high $[Ca^{2+}]_o$ ACSF would increase PPR. On the other hand, the PPR would be decreased by the application of high $[Ca^{2+}]_o$ ACSF in combination with CgTx if the amount of Ca^{2+} influx itself is a critical factor in the CgTx-induced increase in PPR.

Figure 5*A–C* shows an example of the effect of $[Ca^{2+}]_o$ ACSF on PPR. In this case, CgTx (3 μM) decreased the amplitude of the first uIPSCs with less effect on the second uIPSCs, and as a result, the PPR was increased. Under the application of CgTx, an increase in $[Ca^{2+}]_o$ from 2 to 4 mM prominently enhanced both the first and second uIPSCs. In parallel to the enhancement of uIPSC amplitude, the PPR was also increased from 0.57 to 0.83 by application of high $[Ca^{2+}]_o$ (Fig. 5*B*,*C*).

In summary, application of 4 mM $[Ca^{2+}]_o$ with CgTx increased the PPR from 0.59 ± 0.04 in CgTx to 0.70 ± 0.04 in 4 mM $[Ca^{2+}]_o$ with CgTx ($n = 12$; $t_{(11)} = 2.413$, $p = 0.034$, paired t test; Fig. 5*D*). Therefore, the reason for the CgTx-induced increase in the PPR is likely that Ca^{2+} influx via P/Q-type VDCCs serves to yield an increase in PPR, and it is less likely that a decrease in the amount of Ca^{2+} influx via N-type VDCCs increases PPR.

Besides, we examined whether postsynaptic $GABA_A$ receptors were saturated under application of CgTx and 4 mM $[Ca^{2+}]_o$ (Fig. 5*E–I*). Before testing the effects of CgTx, uIPSCs were recorded under application of 4 mM $[Ca^{2+}]_o$, which increases release probability (Fig. 5*E–G*). All of the IPSC amplitudes observed under application of 4 mM $[Ca^{2+}]_o$ were larger than that in both application of CgTx and 4 mM $[Ca^{2+}]_o$ (119.3 ± 23.3 pA in 4 mM $[Ca^{2+}]_o$, 83.6 ± 17.8 pA in CgTx and 4 mM $[Ca^{2+}]_o$, $n = 5$, $t_{(4)} = 2.950$, $p = 0.032$, paired t test; Fig. 5*H*,*I*). These results strongly suggest that $GABA_A$ receptors are not saturated under CgTx and 4 mM $[Ca^{2+}]_o$ application.

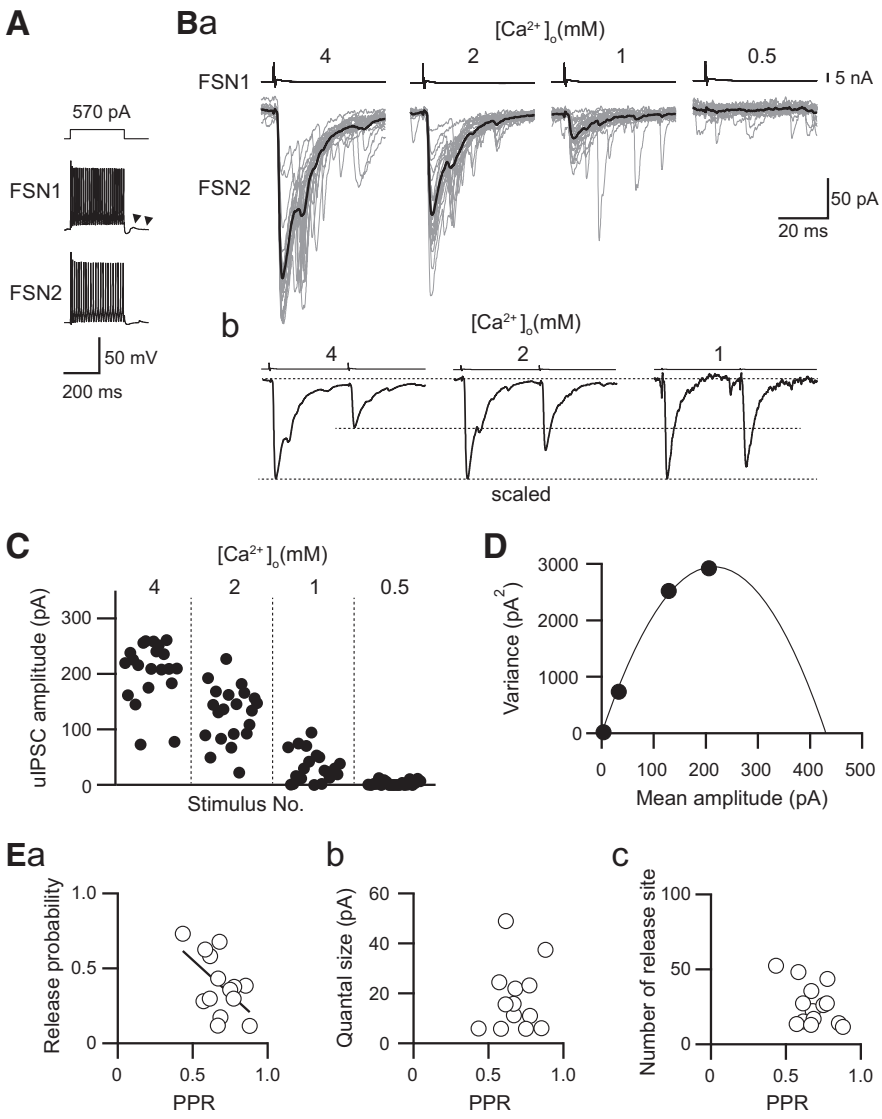

Figure 4. PPR depends on the putative release probability revealed by variance–mean analysis. ***A***, Repetitive firing of presynaptic and postsynaptic FSNs (FSN1 and FSN2, respectively). Autaptic responses were observed just after the end of the depolarizing pulse applied to FSN1 (arrowheads). ***B***, uIPSCs recorded under the application of 4.0, 2.0, 1.0, and 0.5 mM $[Ca^{2+}]_o$ ACSF (***a***). uIPSCs responding to paired-pulse stimulation of the presynaptic FSN1 are shown in ***b***. The amplitudes of the first uIPSCs are scaled. Responses under 0.5 mM $[Ca^{2+}]_o$ are not shown because of their negligible amplitude. ***C***, Distribution of the uIPSC amplitude in response to 0.5–4.0 mM $[Ca^{2+}]_o$ ACSF obtained from 20 consecutive trials. ***D***, Mean uIPSC amplitude and their variance are fitted with a quadratic function. Data were obtained from the same connection between FSN1 and FSN2 as shown in ***A–C***. ***E***, Summary of the relationship between the PPR and putative release probability (***a***), quantal size (***b***), and the number of release sites (***c***). Note a significant correlation between the PPR and release probability ($n = 14$, $r = -0.545$, $p = 0.044$, Pearson correlation).

Increase in PPR by roscovitine by facilitation of P/Q-type and suppression of N-type VDCCs

Roscovitine is known to inhibit cyclin-dependent kinases 1, 2, and 5 and to activate CaV 2 (N-type and P/Q-type) channels by prolonging the open time and increasing the open probability of these channels (Yan et al., 2002; DeStefino et al., 2010; Su et al., 2012; Satake and Imoto, 2014). Thus, we examined the effects of roscovitine (30 μM) on the PPR under the application of VDCC blockers.

Figure 6*A–C* shows an example of roscovitine in combination with 3 μM CgTx on uIPSC amplitude in an FSN→FSN connection. Bath application of CgTx decreased the first uIPSC amplitude with an increase in the PPR (Fig. 6*B*,*C*). Additional application of roscovitine increased the PPR (Fig. 6*B*,*C*). In summary, CgTx suppressed the first uIPSC amplitude from 92.9 ± 17.2 to 72.1 ± 18.6 pA ($n = 13$, $t_{(12)} = 2.715$, $p = 0.019$, paired t test with Bonferroni's correction) but did not have a significant effect on the second uIPSCs (from 55.7 ± 12.6 to 48.5 ± 12.6 pA, $n = 13$, $t_{(12)} = 1.058$, $p = 0.28$, paired t test with Bonferroni's correction). The application of roscovitine in combination with CgTx enhanced the second uIPSCs (48.4 ± 12.7 pA in CgTx; 59.5 ± 11.6 pA in roscovitine with CgTx, $n = 13$; $t_{(12)} = 2.642$, $p = 0.022$, paired t test with Bonferroni's correction) without a significant effect on the first uIPSCs (71.9 ± 18.6 pA in CgTx; 78.1 ± 19.7 in roscovitine with CgTx, $n = 13$; $t_{(12)} = 0.684$, $p =$

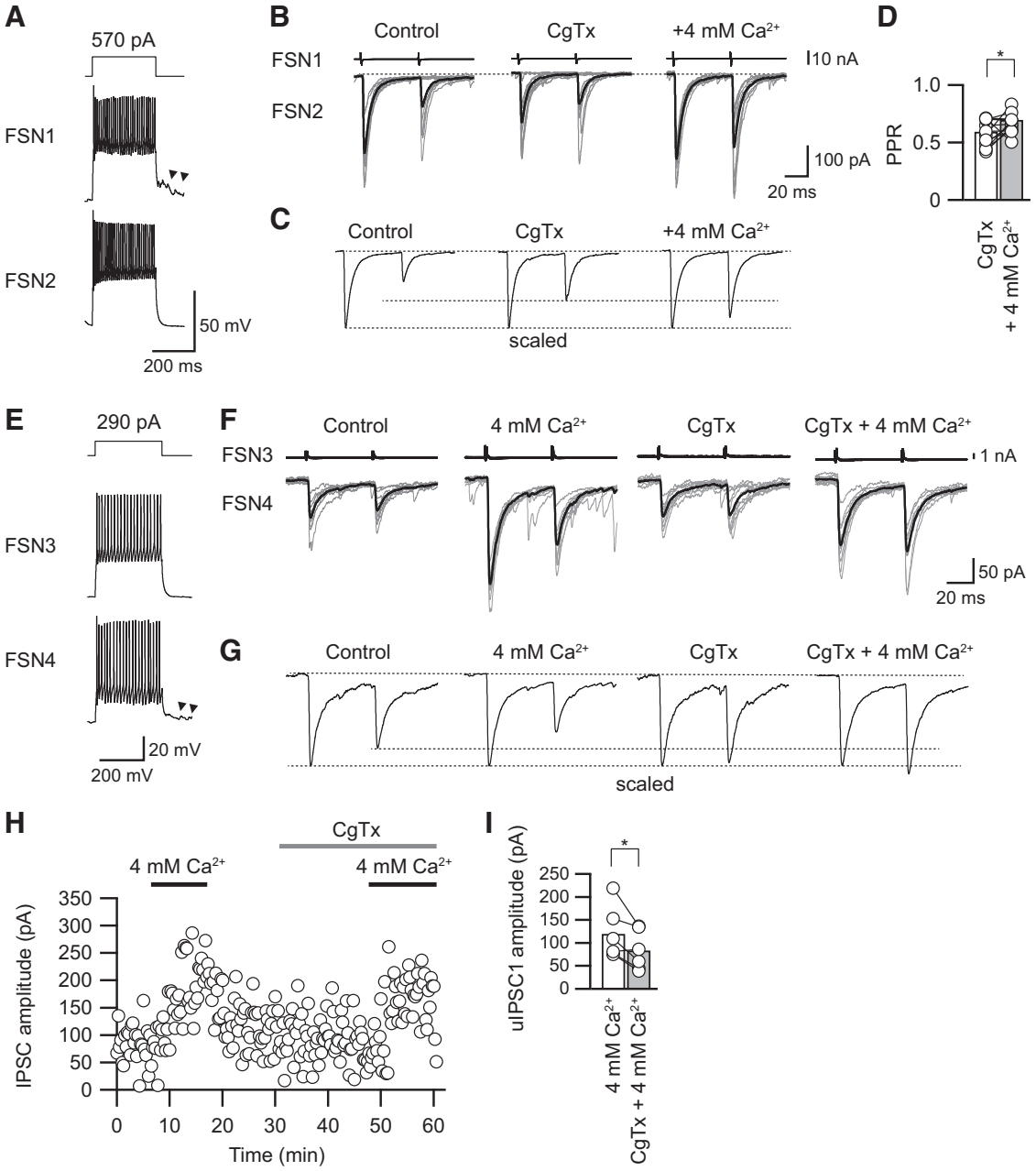

Figure 5. Effects of high $[Ca^{2+}]_o$ on the PPR under application of CgTx. ***A***, Repetitive firing of presynaptic and postsynaptic FSNs (FSN1 and FSN2, respectively). Autaptic responses were observed just after the end of the depolarizing pulse applied to FSN1 (arrowheads). ***B***, Raising $[Ca^{2+}]_o$ to 4 mM under application of CgTx (3 μM) increased the PPR in parallel to an enhancement of both the first and second uIPSCs. ***C***, The averaged uIPSCs obtained from 10 consecutive traces shown in ***B*** were scaled to compare the PPR in the control, during CgTx application, and during CgTX and 4 mM $[Ca^{2+}]_o$ application. Note the enhancement of the PPR by application of CgTx and 4 mM $[Ca^{2+}]_o$. ***D***, Raising $[Ca^{2+}]_o$ to 4 mM significantly increased the PPR ($n = 12$). ***E***, Repetitive firing of presynaptic and postsynaptic FSNs (FSN3 and FSN4, respectively). ***F***, Consecutive traces and their averaged uIPSCs in control and during application of 4 mM $[Ca^{2+}]_o$, CgTx, and CgTx and 4 mM $[Ca^{2+}]_o$. ***G***, The averaged uIPSCs obtained from 10 consecutive traces shown in ***F*** were scaled to compare PPR. ***H***, The time course of uIPSC amplitude shown in ***F***. ***I***, uIPSCs under 4 mM $[Ca^{2+}]_o$ were larger than those under application of CgTx and 4 mM $[Ca^{2+}]_o$ ($n = 5$). *$p < 0.05$, paired *t* test.

0.507, paired *t* test with Bonferroni's correction; Fig. 6*D*). As a result, the PPR was increased from 0.71 ± 0.06 to 0.83 ± 0.06 ($n = 13$) by application of roscovitine in combination with CgTx ($t_{(12)} = 2.182$, $p = 0.049$, paired *t* test; Fig. 6*E*).

In a part of the experiment, uIPSCs were recorded under 4 mM $[Ca^{2+}]_o$ to examine whether postsynaptic $GABA_A$ receptors are saturated by application of CgTx and roscovitine (Fig. 6*F–J*). uIPSCs under application of CgTx and roscovitine were smaller than that in 4 mM $[Ca^{2+}]_o$ (153.4 ± 47.6 pA in 4 mM $[Ca^{2+}]_o$, 65.2 ± 47.6 pA in CgTx and roscovitine, $n = 8$, $t_{(7)} = 3.051$, $p = 0.019$; paired *t* test; Fig. 6*G–J*). Therefore, a facilitative shift of the PPR in the presence of CgTx and roscovitine is unlikely to be caused by saturation of $GABA_A$ receptors (Fig. 6*E*).

In contrast to the effect of roscovitine on P/Q-type VDCCs, Finley et al. (2010) reported the suppression of N-type VDCCs by roscovitine. In agreement with their observations, roscovitine likely acted as an inhibitor of N-type VDCCs in FSN→FSN/non-FSN connections: roscovitine completely blocked uIPSCs mediated by N-type VDCCs that were isolated by application of AgTx (Fig. 7*A*,*B*). Overall, roscovitine suppressed uIPSC amplitude under the application of AgTx from 12.5 ± 2.2 to 3.6 ± 4.3 pA ($n = 8$, $t_{(7)} = 5.724$, $p = 0.001$, paired *t* test; Fig. 7*C*).

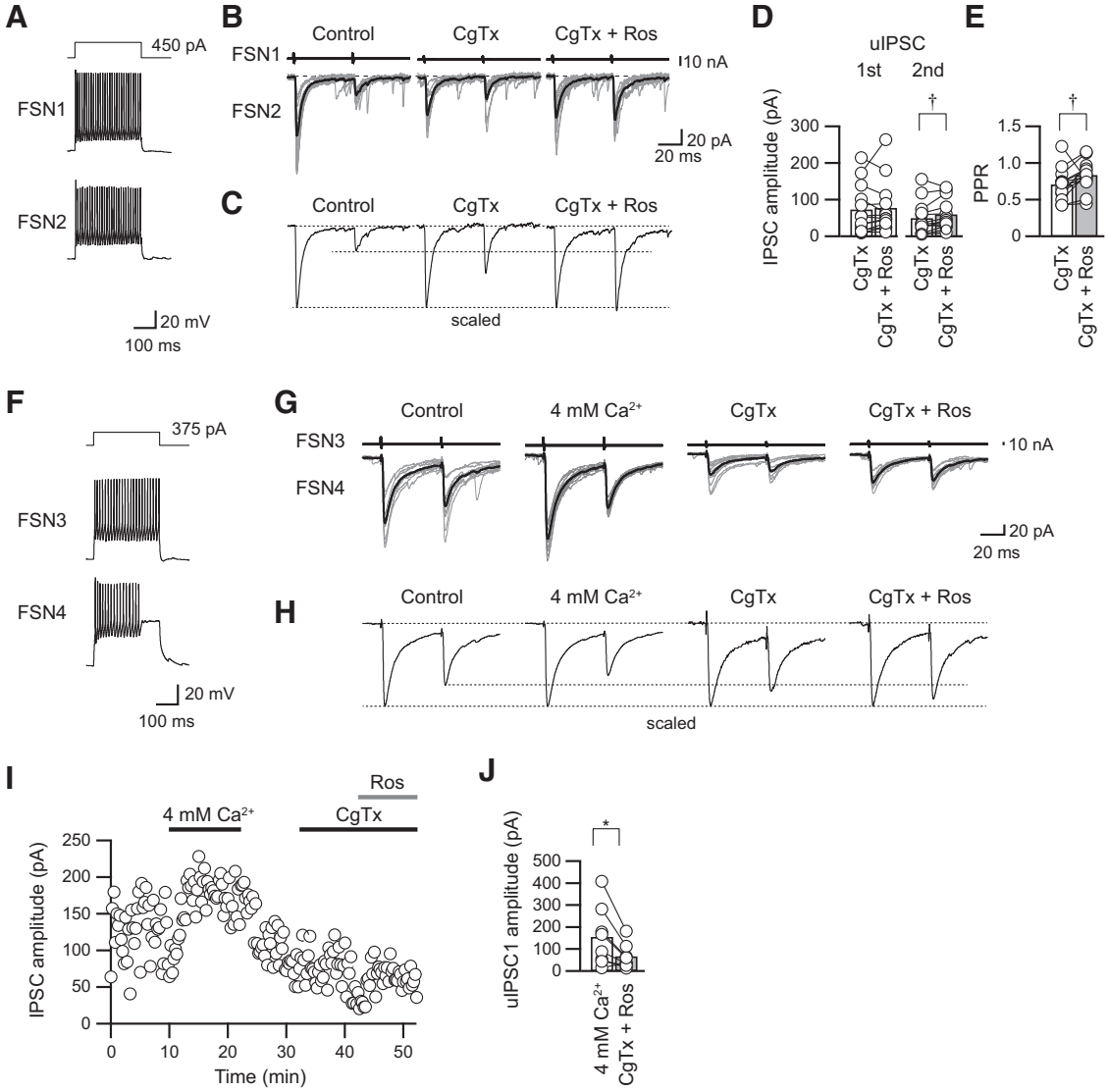

Figure 6. Effects of roscovitine in combination with CgTx on uIPSC amplitude and PPR. ***A***, Repetitive firing of presynaptic FSN1 and FSN2. ***B***, Ten consecutive traces (gray) with averaged traces (black) before (control), during CgTx (3 μM) application, and with additional application of roscovitine (CgTx and Ros; 30 μM). ***C***, Scaled uIPSCs showing an increase in PPR. ***D***, ***E***, Summary of the effects of roscovitine on uIPSC amplitude and PPR in the presence of CgTx ($n = 13$). The second but not the first uIPSCs were enhanced by roscovitine (***D***). As a result, the PPR was increased by roscovitine (***E***). ***F***, Repetitive firing of presynaptic and postsynaptic FSNs (FSN2 and FSN3, respectively). ***G***, Consecutive traces and their averaged uIPSCs in control and during application of 4 mM $[Ca^{2+}]_o$, CgTx, and CgTx and roscovitine. ***H***, The averaged uIPSCs obtained from 10 consecutive traces shown in ***G*** were scaled to compare the PPR. ***I***, The time course of uIPSC amplitude shown in ***G***. ***J***, uIPSCs under 4 mM $[Ca^{2+}]_o$ were larger than those under application of CgTx and roscovitine ($n = 8$). $^{\dagger}p < 0.05$, paired t test with Bonferroni's correction; $^{*}p < 0.05$, paired t test.

If roscovitine potentiates and suppresses P/Q-type and N-type VDCCs, respectively, roscovitine itself would increase the PPR. Figure 8*A–C* shows an example of the effect of roscovitine on paired uIPSCs. As presumed above, roscovitine increased the PPR with an increase in the second uIPSC amplitude. In summary, administration of roscovitine alone increased the second uIPSC amplitude (34.2 ± 6.1 to 43.4 ± 7.7 pA, $n = 18$, $t_{(17)} = 3.150$, $p = 0.006$, paired t test; Fig. 8*D*) without an effect on the first uIPSC amplitude (53.3 ± 10.8 to 58.6 ± 13.0 pA, $n = 18$, $t_{(17)} = 1.022$, $p = 0.321$, paired t test). As a result, the PPR in-

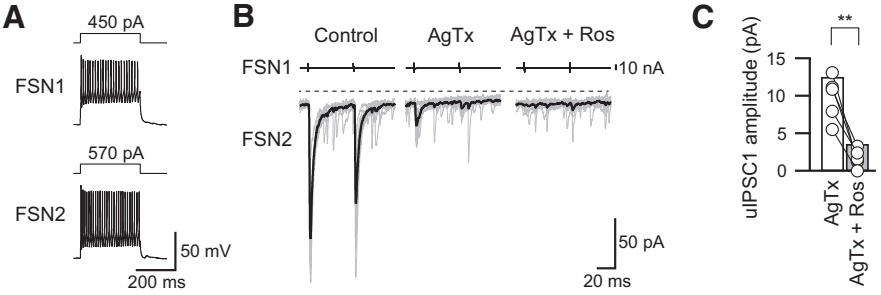

Figure 7. Roscovitine attenuated the N-type VDCC component of uIPSCs isolated by AgTx. ***A***, Repetitive firing of presynaptic and postsynaptic FSNs (FSN1 and FSN2, respectively). ***B***, Effects of roscovitine (Ros; 30 μM) on the remaining uIPSC component in the FSN1→FSN2 connection after administration of AgTx (200 nM). ***C***, Summary of the first uIPSC amplitude diminished by roscovitine in the presence of AgTx ($n = 8$). $^{**}p < 0.01$, paired t test.

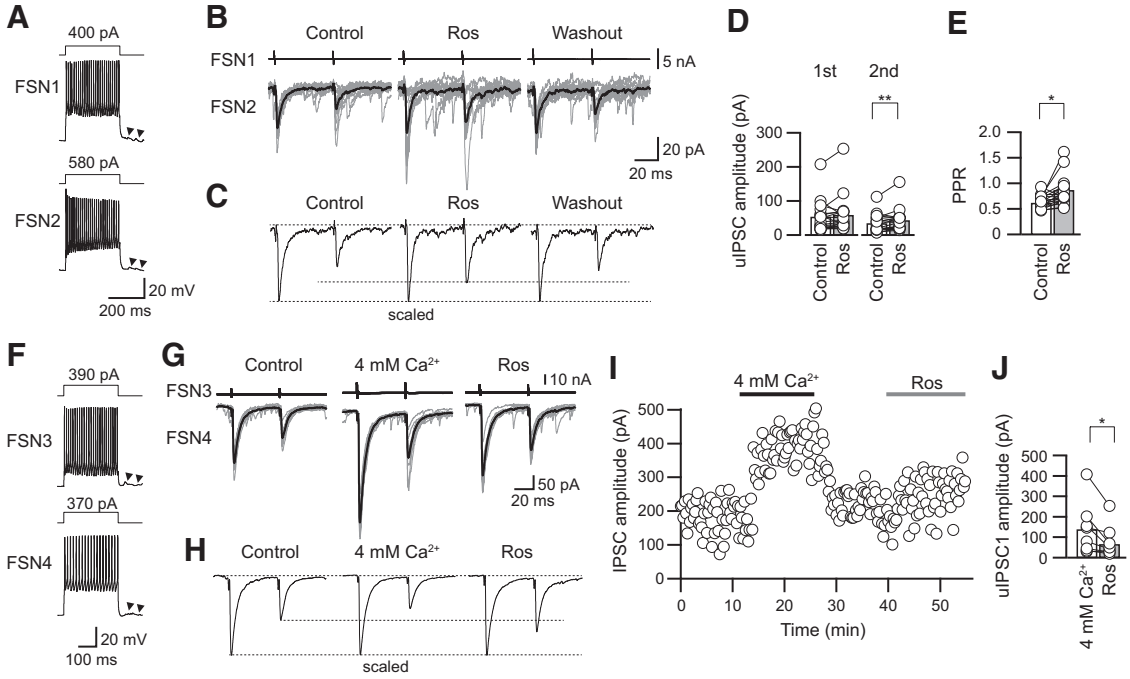

Figure 8. Roscovitine increased the second uIPSC amplitude. ***A***, Repetitive firing of presynaptic and postsynaptic FSNs (FSN1 and FSN2, respectively). Arrowheads indicate autaptic responses. ***B***, Effects of roscovitine (Ros; 30 μM) on uIPSCs in the FSN1→FSN2 connection. ***C***, Scaled traces before roscovitine treatment (Control), during application of roscovitine (Ros), and after washout of roscovitine. ***D***, ***E***, Facilitative effects of roscovitine on the second uIPSC amplitude (***D***) and PPR ($n = 18$; ***E***). ***F***, Repetitive firing of presynaptic and postsynaptic FSNs (FSN3 and FSN4, respectively). ***G***, Consecutive traces and their averaged uIPSCs in control and during application of 4 mM $[Ca^{2+}]_o$, CgTx, and roscovitine. ***H***, The averaged uIPSCs obtained from 10 consecutive traces shown in ***G*** were scaled to compare the PPR. ***I***, The time course of uIPSC amplitude shown in ***G***. ***J***, uIPSCs under 4 mM $[Ca^{2+}]_o$ were larger than those under application of roscovitine ($n = 8$). *$p < 0.05$; **$p < 0.01$, paired *t* test.

creased from 0.66 ± 0.03 to 0.82 ± 0.07 ($n = 18$, $t_{(17)} = 2.576$, $p = 0.020$, paired *t* test; Fig. 8*E*).

Similar to Figure 6*F–J*, uIPSCs were recorded under 4 mM $[Ca^{2+}]_o$ to examine whether postsynaptic $GABA_A$ receptors are saturated by application of roscovitine (Fig. 8*F–J*). uIPSC amplitude during application of 4 mM $[Ca^{2+}]$ and roscovitine were 138.0 ± 44.7 and 65.3 ± 21.9 pA, respectively ($n = 8$, $t_{(7)} = 2.823$, $p = 0.026$, paired *t* test; Fig. 8*G–J*), suggesting that the increase in the PPR by roscovitine is unlikely to be caused by saturation of $GABA_A$ receptors (Fig. 8*E*).

Blockade of Ca^{2+}-dependent K^+ efflux attenuates AgTx-induced suppression of PPR

VDCCs play a pivotal role in neurotransmitter release, and Ca^{2+} influx via VDCCs often activates K_{Ca} channels, which hyperpolarize the membrane potential. K_{Ca} channels are classified into three types, i.e., BK, IK, and SK channels, which have large, intermediate, and small conductances, respectively (Berkefeld et al., 2010). Some K_{Ca} channels are expressed on presynaptic and postsynaptic membranes and regulate spike firing and synaptic transmission (Kobayashi et al., 1997; Marrion and Tavalin, 1998; Wikström and El Manira, 1998). In particular, BK channels have been reported to couple with several types of VDCCs not only in somata but also in axon terminals (Goldberg et al., 2005; Fakler and Adelman, 2008). Thus, there is a possibility that Ca^{2+} influx via N-type VDCCs may activate K_{Ca} channels in the presynaptic terminals of FSN, which may suppress GABA release. To test this possibility, we examined whether K_{Ca} channels activated by Ca^{2+} influx through N-type VDCCs in the terminal modulate uIPSC amplitude and induce associated changes in PPR.

First, we measured the half-widths of the first and second action potentials in FSNs during the application of ChTx (50–100 nM), a BK and IK channel blocker, and apamin (1 μM), an SK channel blocker (Fig. 9). This is because blockade of K_{Ca} channels may prolong the duration of action potentials and induce longer activation of VDCCs. If so, it is likely that these blockers induce larger Ca^{2+} influx and increase release probability. Representative examples of the effects of AgTx and ChTx with AgTx are shown in Figure 9*A*, and those of AgTx and apamin with AgTx are shown in Figure 9*B*. AgTx application had little effect on the half-width of the first and second action potentials (first action potential, 1.14 ± 0.07 ms, second action potential, 1.17 ± 0.07 ms, $n = 16$, $t_{(15)} = 1.261$, $p = 0.227$, paired *t* test; Fig. 9*C*). Similarly, ChTx with AgTx and apamin with AgTx had little effect on spike duration (ChTx: first action potential, 1.13 ± 0.10 ms; second action potential, 1.15 ± 0.11 ms; $n = 8$, $t_{(7)} = 1.873$, $p = 0.103$, paired *t* test; apamin, first action potential, 1.11 ± 0.11 ms; second action potential, 1.12 ± 0.10 ms; $n = 5$, $t_{(4)} = 0.278$, $p = 0.795$, paired *t* test; Figure 9*C*). There was no significant difference in the half-durations of the first and second action potentials among the control, AgTx, ChTx with AgTx, and apamin with AgTx (first action potential, $F_{(3,41)} = 0.078$, $p = 0.971$; second action potential, $F_{(3,41)} = 0.071$, $p = 0.975$, one-way ANOVA). Therefore, it is likely that the suppressive effect of the PPR by Ca^{2+} influx through N-type VDCCs is not attributable to the change in duration of action potential in presynaptic FSNs.

Next, we examined the effects of ChTx alone and in combination with AgTx, which extracts synaptic currents through N-type VDCCs (Fig. 10). No significant change in the PPR was observed under the condition in which ChTx was added in normal ACSF (Fig. 10*A–C*): 0.81 ± 0.07 in the control and 0.74 ± 0.10 with ChTx application ($n = 7$; $t_{(6)} = 1.042$, $p = 0.337$, paired *t* test; Fig. 10*D*). In contrast, the PPR of uIPSCs was increased by ChTx under application of AgTx accompanying with a suppressive ten-

dency of uIPSCs that were mediated by N-type VDCCs (Fig. 10*E–I*): $IPSC_1$, 23.4 ± 4.7 pA under application of AgTx and 10.8 ± 2.5 pA ($n = 10$; $t_{(9)} = 2.146$, $p = 0.060$, paired *t* test); $IPSC_2$, 16.2 ± 4.1 pA under application of AgTx and 10.0 ± 1.6 pA ($n = 10$; $t_{(9)} = 1.933$, $p = 0.085$, paired *t* test; Fig. 10*H*); PPR, 0.68 ± 0.11 with AgTx application and 0.97 ± 0.09 with application of ChTx and AgTx ($n = 10$; $t_{(9)} = 2.420$, $p = 0.039$, paired *t* test; Fig. 10*I*).

Similar to the small effect of ChTx on PPR, apamin alone had little effect on the PPR by itself [Fig. 11*A–C*, 0.84 ± 0.10 in control and 0.68 ± 0.11 ($n = 7$; $t_{(6)} = 1.157$, $p = 0.291$, paired *t* test); Fig. 11*D*]. However, apamin increased the PPR accompanying a tendency of decreases in amplitude under preapplication of AgTx (Fig. 11*E–I*): $IPSC_1$, 38.0 ± 14.4 pA under application of AgTx and 14.6 ± 2.9 pA ($n = 7$; $t_{(6)} = 1.924$, $p = 0.103$, paired *t* test); $IPSC_2$, 18.9 ± 8.4 pA under application of AgTx and 14.69 ± 4.30 pA ($n = 7$; $t_{(6)} = 0.784$, $p = 0.463$, paired *t* test; Fig. 11*H*); PPR, 0.50 ± 0.09 under application of AgTx and 0.92 ± 0.10 under application of apamin and AgTx ($n = 7$; $t_{(6)} = 2.742$, $p = 0.034$, paired *t* test; Fig. 11*I*).

These results suggest an involvement of K_{Ca} channels in AgTx-induced suppression of PPR, and this effect has little selectivity among K_{Ca} channel subtypes.

Discussion

In FSN→FSN/non-FSN connections, each projection from a common presynaptic FSN to different postsynaptic GABAergic neurons showed distinct short-term plasticity and discrete sensitivity to P/Q-type and N-type VDCC blockers, which suppressed and facilitated PPR, respectively. N-type VDCC-mediated PPR suppression was blocked by ChTx or apamin, suggesting that Ca^{2+} influx through N-type VDCCs suppresses the PPR by activating K_{Ca} channels. These results suggest that the expression pattern of VDCCs in the GABAergic synaptic terminals is not homogenously organized even if these terminals are branched from a common presynaptic neuron, and such divergent expression of VDCC subtypes makes it possible to regulate short-term plasticity precisely in each inhibitory connection.

Expression profiles of N- and P/Q-type VDCCs in GABAergic synaptic terminals

PPR of uIPSCs between presynaptic FSN and postsynaptic GABAergic interneurons showed wide variation even with a

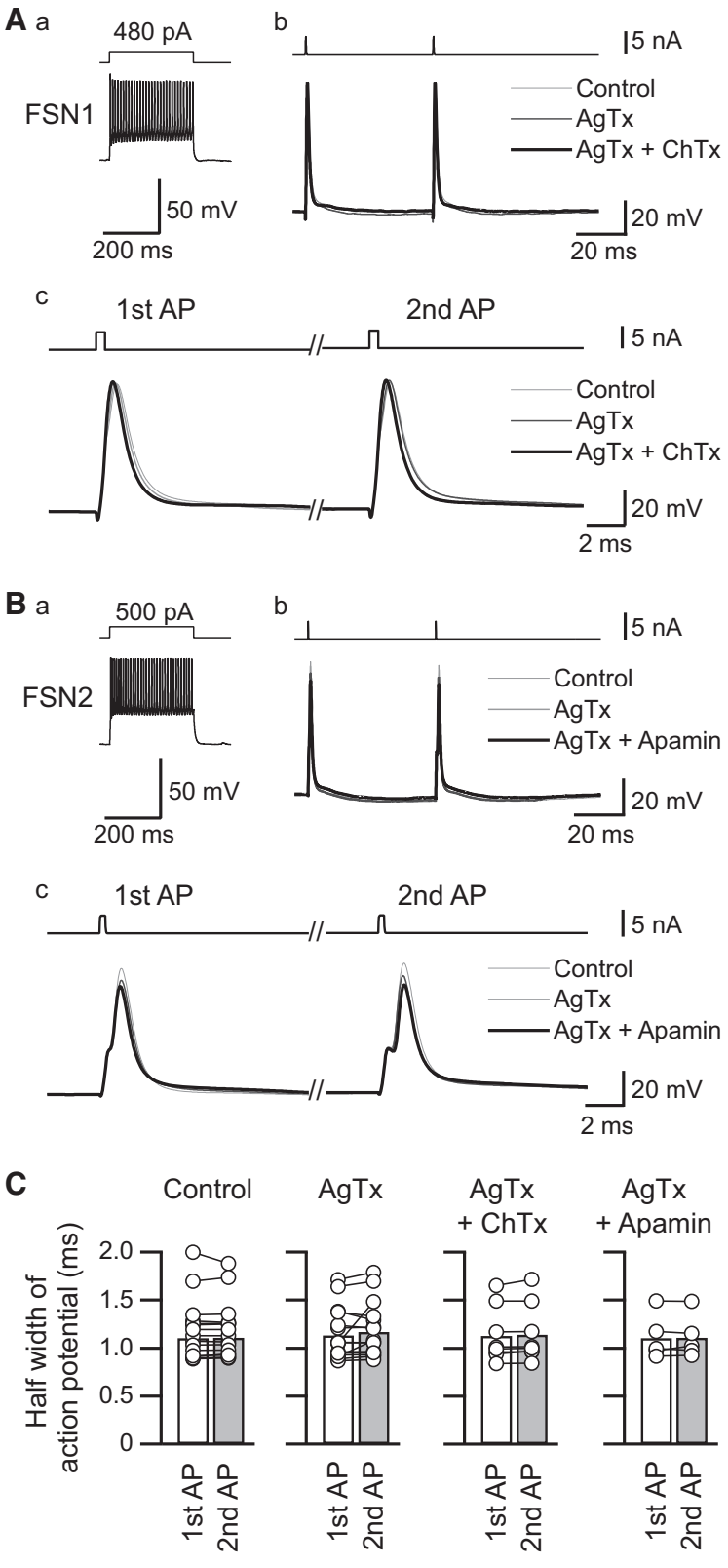

Figure 9. Effects of Ca^{2+}-dependent K^+ channel blockers, charybdotoxin (ChTx, ***A***), and apamin (***B***) on the kinetics of action potential of FSNs. ***Aa***, ***Ba***, Repetitive firing induced by a depolarizing pulse (300 ms) to the FSNs. ***Ab***, ***Bb***, Representative action potentials under control conditions and during application of AgTx with and without ChTx (***A***) or apamin (***B***). Action potentials were evoked from resting membrane potential (ChTx, −65 mV; apamin, −60 mV) by injection of short depolarizing current pulses (0.5 ms, bottom trace) at a 50 ms interstimulus interval. ***Ac***, ***Bc***, Time-expanded traces of the first and second action potentials. Although apamin in combination with AgTx slightly decreased the peaks of the first and second action potentials, little change was observed in action potential duration with ChTx and apamin. ***C***, Summary of the effects of ChTx ($n = 8$) and apamin ($n = 5$) on the half-width of the first and second action potentials under application of AgTx ($n = 16$).

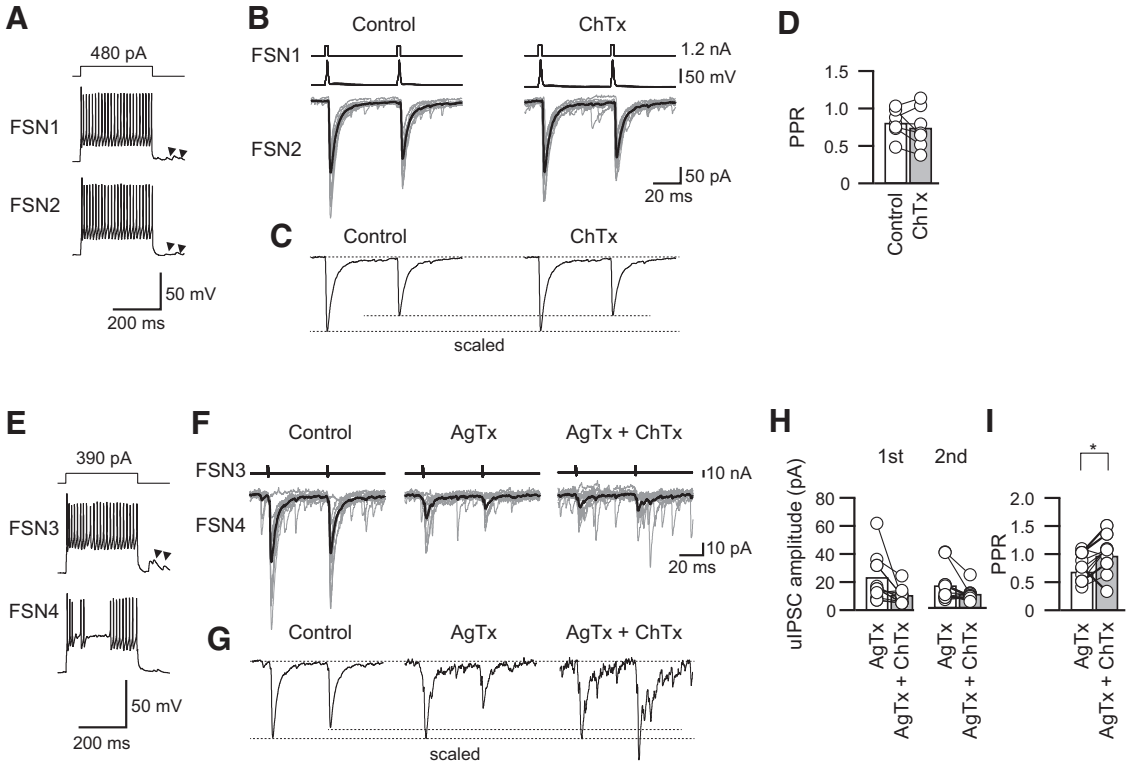

Figure 10. Effects of ChTx with and without AgTx on PPR. ***A***, Repetitive firing of presynaptic and postsynaptic FSNs (FSN1 and FSN2, respectively). Arrowheads indicate autaptic responses. ***B***, ***C***, Ten consecutive traces (gray) with averaged traces (black; ***B***) and the scaled traces (***C***) in the control and during ChTx application. ***D***, ChTx alone induced little change in the PPR ($n = 7$). ***E***, Repetitive firing of presynaptic and postsynaptic FSNs (FSN3 and FSN4, respectively). ***F***, Effects of ChTx on uIPSCs in the presence of AgTx in the FSN3→FSN4 connection shown in ***E***. ***G***, Scaled traces in the control condition and during application of AgTx without and with ChTx. Note the facilitative effect of ChTx on the PPR. ***H***, uIPSC amplitude during AgTx and AgTx and ChTx ($n = 10$). ***I***, ChTx with AgTx facilitated the PPR ($n = 10$). *$p < 0.05$, paired *t* test.

shared presynaptic FSN. Such target-cell-specific profiles of short-term plasticity have been reported in glutamatergic synapses in the cerebral cortex (Reyes et al., 1998; Rozov et al., 2001; Koester and Johnston, 2005). A presynaptic pyramidal neuron induces paired-pulse depression in connection with multipolar cells and paired-pulse facilitation in connection with bitufted cells. The present study did not identify the immunohistochemical features of the recorded neurons such as somatostatin-, vasoactive intestinal peptide-, and calbindin-immunopositive neurons (Kawaguchi and Kubota, 1997). The immunohistochemical variation of neural subtypes might be responsible for the heterogeneity of VDCC expression; however, cell classification according to electrophysiological properties did not show consistency between the PPR and postsynaptic neuronal subtypes. We thus found that not only glutamatergic pyramidal neurons but also GABAergic FSNs show a distinct PPR for each connection and extended that finding by demonstrating that individual connections between GABAergic neurons often exhibit different sensitivities to N- and P/Q-type VDCC blockers. The difference in uIPSC sensitivities to VDCC blockers indicates that each synaptic terminal shows its own expression pattern of VDCC subtypes.

Synaptic short-term plasticity depends on VDCC subtypes expressed in the terminal

The expression profiles of VDCC subtypes in synaptic terminals have been studied in various brain regions. Takahashi and Momiyama (1993) reported that in the hippocampal CA1 region, EPSCs evoked by Schaffer collateral stimulation are partially attenuated by CgTx application and that the remaining component is completely blocked by AgTx, demonstrating that N- and P/Q-type VDCCs colocalize in Schaffer collateral terminals. In contrast to hippocampal synapses coexpressing N- and P/Q-type VDCCs, presynaptic FSNs and postsynaptic pyramidal neurons in neocortical slice preparations show uIPSCs that are completely blocked by AgTx (Zaitsev et al., 2007). Among these studies, we primarily demonstrated the distinct short-term plasticity in the connections between GABAergic neurons in the cerebral cortex: Ca^{2+} influx through P/Q-type VDCCs increased PPR, whereas that through N-type VDCCs decreased PPR. Taking advantage of using VGAT-Venus transgenic rats and a multiple whole-cell patch-clamp technique, we compared short-term plasticity in the GABAergic connections that consisted of a common presynaptic FSN and excluded the possibility that different properties of short-term plasticity are attributable to presynaptic neuron subtypes. In contrast to FSN→FSN/non-FSN connections in IC, EPSCs evoked by stimulation of Shaffer collaterals in the hippocampal CA1 region show suppressed and enhanced PPRs after application of CgTx and AgTx, respectively (Scheuber et al., 2004). This discrepancy may be attributed to distinct profiles of glutamate and GABA release by activating VDCC subtypes.

We did not clarify whether N-type and P/Q-type VDCCs are coexpressed or separately expressed in each GABAergic synapse. Unless either CgTx or AgTx completely abolished uIPSCs, two possibilities remain: (1) a subset of synapses express only N-type or P/Q-type channels or (2) both VDCC subtypes are coexpressed in a synapse. In the active zone of glutamatergic terminals arising from hippocampal CA3 pyramidal neurons, both N-type and P/Q-type VDCCs are detected, and their numbers have been counted by immunoelectron microscopy, suggesting that the lat-

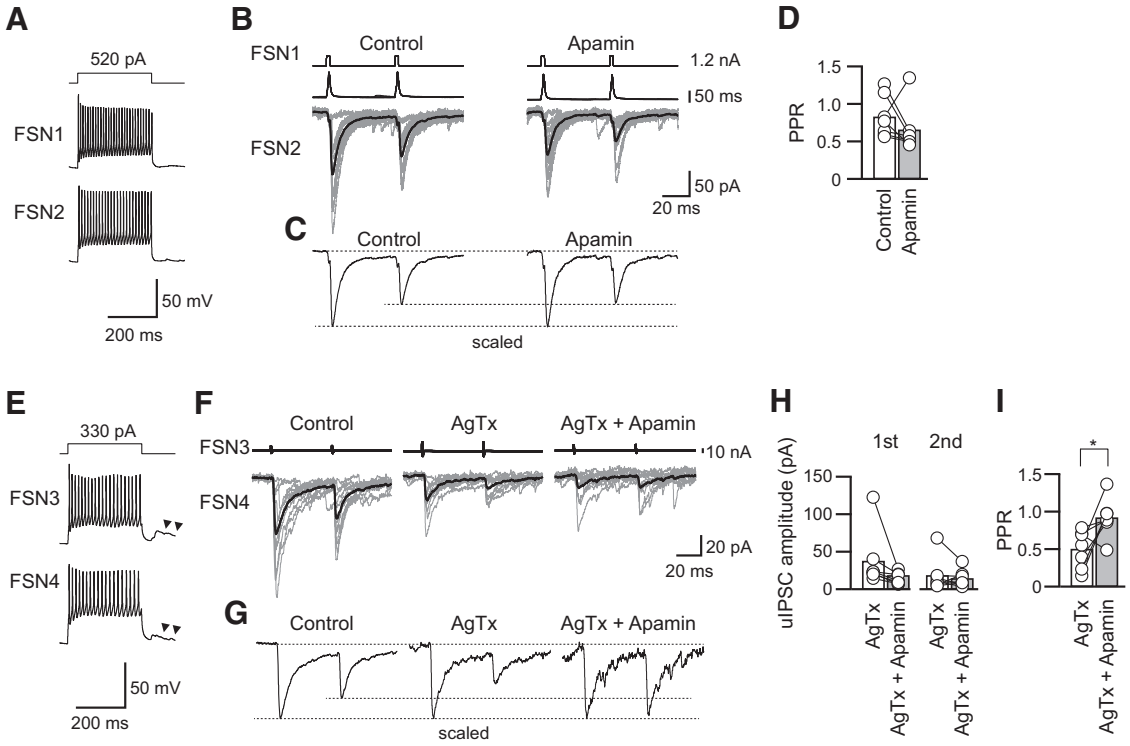

Figure 11. Effects of apamin with and without AgTx on PPR. ***A***, Repetitive firing of presynaptic (FSN1) and postsynaptic (FSN2) FSNs. ***B***, ***C***, Ten consecutive traces (gray) with averaged traces (black; ***B***) and the scaled traces (***C***) in the control and during apamin application. ***D***, Apamin had little effect on the PPR ($n = 7$). ***E***, Repetitive firing of presynaptic (FSN3) and postsynaptic (FSN4) FSNs. Arrowheads indicate autaptic responses. ***F***, Effects of apamin on uIPSCs in the presence of AgTx in the FSN3→FSN4 connection shown in ***E***. ***G***, Scaled traces in the control and during application of AgTx without and with apamin. Note the facilitative effect of apamin with AgTx on the PPR. ***H***, uIPSC amplitude during AgTx and AgTx and apamin ($n = 7$). ***I***, Apamin facilitated the PPR in the presence of AgTx ($n = 7$). $^*p < 0.05$, paired *t* test.

ter possibility is likely (Éltes et al., 2017). This expression pattern might also apply to GABAergic synapses.

Mechanisms for short-term plasticity regulated by VDCCs

BK and SK channels are expressed in the soma, axon initial segment, and synaptic terminal in the neuron (Kobayashi et al., 1997; Fakler and Adelman, 2008). In this study, the attenuation of the PPR by application of AgTx was blocked by administration of K_{Ca} channel blockers, suggesting that hyperpolarization induced by activation of K_{Ca} channels in GABAergic synaptic terminals of FSNs is among the mechanisms underlying the induction of low PPR. Indeed, single-cell multiplex RT-PCR of rat neocortical neurons in combination with electrical recording demonstrated not only coexpression of N-type and P/Q-type VDCCs but also expression of the gene for SK channels in the single parvalbumin-expressing neuron, which is presumably an FSN (Toledo-Rodriguez et al., 2004). K_{Ca} blockers tended to decrease N-type VDCC-mediated uIPSCs, consistent with the previous report that presynaptic BK channels increase transmitter release via unknown mechanisms (Pattillo et al., 2001). This unknown mechanism should be explored further.

In hippocampal mossy fiber synapses, P/Q-type VDCCs generate homogeneous elevation of $[Ca^{2+}]_i$, whereas N-type VDCCs induce highly localized Ca^{2+} elevation, and these are mechanisms of distinct roles in short-term plasticity (Chamberland et al., 2017). If this is the case in GABAergic terminals of IC FSNs, it is likely that N-type VDCCs and K_{Ca} channels are located in close spatial proximity in GABAergic synaptic terminals, as previously suggested (Kobayashi et al., 1997). It was also reported that synaptic response and PPR are influenced by the application of BK and SK channel blockers (Raffaelli et al., 2004; Berkefeld et al., 2010; Griguoli et al., 2016). Under the application of a BK channel blocker, iberiotoxin, prolongation of the half-duration of action potentials occurs in the soma and the axon initial segment of the cortical pyramidal neuron, which may result in an increase in Ca^{2+} influx and in transmitter release at the presynaptic terminals. However, this is not the case in our preparation because spike width was not changed by K_{Ca} channel blockers.

It is commonly assumed that the mechanisms underlying paired-pulse depression and facilitation are depletion and accumulation, respectively, of residual Ca^{2+} in the synaptic terminal (Blitz et al., 2004). Molecular mechanisms for short-term plasticity have been studied in detail in the cholinergic synaptic connections among cultured SCG neurons transfected with brain-derived P/Q-type VDCCs (Mochida et al., 2008; Mori et al., 2014). SCG synapses show paired-pulse depression at interstimulus intervals of <100 ms, whereas a facilitative shift in the PPR is induced at interstimulus intervals of 100–200 ms, suggesting that short-term plasticity depends on the temporal binding interaction of Ca^{2+} entered through P/Q-type VDCCs to Ca^{2+} sensor proteins. In contrast, synaptic connections among SCG neurons expressing N-type VDCCs show synaptic depression at 15–120 ms intervals, and the synaptic depression is attenuated by EGTA-AM and BAPTA-AM, a slow and a rapid Ca^{2+} chelator, respectively. These results indicate that N-type VDCCs suppress the second release, presumably by unknown chelators (Mori et al., 2014). In addition, according to previous work using knockout mice for parvalbumin, a slow Ca^{2+} chelator protein expressed abundantly in FSNs, parvalbumin potently modulates short-term plasticity in presynaptic terminals of FSNs (Caillard et

al., 2000). A detailed investigation of intracellular mechanisms for short-term plasticity in GABAergic synapses should be further conducted to elucidate whether the different distributions of these Ca^{2+}-associating proteins in each terminal contribute to the induction of distinct plasticities, as shown in the present study.

Functional roles of short-term plasticity in GABAergic neuronal connections

The profiles of short-term plasticity might reflect the mechanisms of long-term synaptic plasticity, as demonstrated in the connections from presynaptic pyramidal cells to postsynaptic GABAergic neurons (Lu et al., 2007). The connections from pyramidal cells to FSNs, which exhibit short-term depression, show long-term depression induced by repetitive correlated spiking. In contrast, the connections from pyramidal cells to low-threshold spiking cells showing short-term facilitation induce long-term potentiation or depression that depends on the timing of presynaptic spikes. Although the induction mechanisms for long-term plasticity are different between glutamatergic and GABAergic synapses, different kinetics of short-term plasticity between GABAergic neurons may contribute to the characterization of plastic changes in response to disturbances of bottom-up signals from the peripheral nervous system.

In the anterior cingulate and barrel cortices, thalamocortical axons project directly to GABAergic interneurons (Porter et al., 2001; Delevich et al., 2015). Among these interneurons, FSNs seem to receive strong excitatory inputs from the thalamus compared with surrounding pyramidal neurons (Cruikshank et al., 2007). Monosynaptic and disynaptic EPSC and IPSC recordings from cortical neurons evoked by thalamic stimulation using thalamocortical slice preparations suggest that inhibitory interneurons are prevented from firing multiple spikes by disynaptic inhibition at a short latency mediated by other inhibitory interneurons in the barrel column (Porter et al., 2001). Part of the functional importance of short-term plasticity in the GABAergic circuit is the filtration of excitatory information by direct inhibition to excitatory neurons and/or indirect regulation of pyramidal neurons by disinhibition of the activities of excitatory neurons (Fortune and Rose, 2001; Abbott and Regehr, 2004). Therefore, the differences in short-term plasticity in FSN→FSN/non-FSN connections may contribute to fine regulation of disinhibition of pyramidal neuronal activities by different expression patterns of N-type and P/Q-type VDCCs at the synaptic terminals of FSNs.

References

Abbott LF, Regehr WG (2004) Synaptic computation. Nature 431:796–803. CrossRef Medline

Ali AB, Nelson C (2006) Distinct Ca^{2+} channels mediate transmitter release at excitatory synapses displaying different dynamic properties in rat neocortex. Cereb Cortex 16:386–393. CrossRef Medline

Almado CE, Machado BH, Leão RM (2012) Chronic intermittent hypoxia depresses afferent neurotransmission in NTS neurons by a reduction in the number of active synapses. J Neurosci 32:16736–16746. CrossRef Medline

Atluri PP, Regehr WG (1996) Determinants of the time course of facilitation at the granule cell to Purkinje cell synapse. J Neurosci 16:5661–5671. CrossRef Medline

Augustine GJ, Charlton MP, Smith SJ (1985) Calcium entry and transmitter release at voltage-clamped nerve terminals of squid. J Physiol 367:163–181. CrossRef Medline

Bellingham MC, Walmsley B (1999) A novel presynaptic inhibitory mechanism underlies paired pulse depression at a fast central synapse. Neuron 23:159–170. CrossRef Medline

Berkefeld H, Fakler B, Schulte U (2010) Ca^{2+}-activated K^+ channels: from protein complexes to function. Physiol Rev 90:1437–1459. CrossRef Medline

Blitz DM, Foster KA, Regehr WG (2004) Short-term synaptic plasticity: a comparison of two synapses. Nat Rev Neurosci 5:630–640. CrossRef Medline

Brown JT, Randall A (2005) Gabapentin fails to alter P/Q-type Ca^{2+} channel-mediated synaptic transmission in the hippocampus in vitro. Synapse 55:262–269. CrossRef Medline

Caillard O, Moreno H, Schwaller B, Llano I, Celio MR, Marty A (2000) Role of the calcium-binding protein parvalbumin in short-term synaptic plasticity. Proc Natl Acad Sci U S A 97:13372–13377. CrossRef Medline

Chamberland S, Evstratova A, Tóth K (2017) Short-term facilitation at a detonator synapse requires the distinct contribution of multiple types of voltage-gated calcium channels. J Neurosci 37:4913–4927. CrossRef Medline

Counotte DS, Goriounova NA, Li KW, Loos M, van der Schors RC, Schetters D, Schoffelmeer AN, Smit AB, Mansvelder HD, Pattij T, Spijker S (2011) Lasting synaptic changes underlie attention deficits caused by nicotine exposure during adolescence. Nat Neurosci 14:417–419. CrossRef Medline

Cruikshank SJ, Lewis TJ, Connors BW (2007) Synaptic basis for intense thalamocortical activation of feedforward inhibitory cells in neocortex. Nat Neurosci 10:462–468. CrossRef Medline

Delevich K, Tucciarone J, Huang ZJ, Li B (2015) The mediodorsal thalamus drives feedforward inhibition in the anterior cingulate cortex via parvalbumin interneurons. J Neurosci 35:5743–5753. CrossRef Medline

DeStefino NR, Pilato AA, Dittrich M, Cherry SV, Cho S, Stiles JR, Meriney SD (2010) (R)-roscovitine prolongs the mean open time of unitary N-type calcium channel currents. Neuroscience 167:838–849. CrossRef Medline

Dunlap K, Luebke JI, Turner TJ (1995) Exocytotic Ca^{2+} channels in mammalian central neurons. Trends Neurosci 18:89–98. CrossRef Medline

Éltes T, Kirizs T, Nusser Z, Holderith N (2017) Target cell type-dependent differences in Ca^{2+} channel function underlie distinct release probabilities at hippocampal glutamatergic terminals. J Neurosci 37:1910–1924. CrossRef Medline

Fakler B, Adelman JP (2008) Control of K_{Ca} channels by calcium nano/microdomains. Neuron 59:873–881. CrossRef Medline

Finley MF, Lubin ML, Neeper MP, Beck E, Liu Y, Flores CM, Qin N (2010) An integrated multiassay approach to the discovery of small-molecule N-type voltage-gated calcium channel antagonists. Assay Drug Dev Technol 8:685–694. CrossRef Medline

Fortune ES, Rose GJ (2001) Short-term synaptic plasticity as a temporal filter. Trends Neurosci 24:381–385. CrossRef Medline

Galarreta M, Hestrin S (2002) Electrical and chemical synapses among parvalbumin fast-spiking GABAergic interneurons in adult mouse neocortex. Proc Natl Acad Sci U S A 99:12438–12443. CrossRef Medline

Goldberg EM, Watanabe S, Chang SY, Joho RH, Huang ZJ, Leonard CS, Rudy B (2005) Specific functions of synaptically localized potassium channels in synaptic transmission at the neocortical GABAergic fast-spiking cell synapse. J Neurosci 25:5230–5235. CrossRef Medline

Griguoli M, Sgritta M, Cherubini E (2016) Presynaptic BK channels control transmitter release: physiological relevance and potential therapeutic implications. J Physiol 594:3489–3500. CrossRef Medline

Horne AL, Kemp JA (1991) The effect of ω-conotoxin GVIA on synaptic transmission within the nucleus accumbens and hippocampus of the rat *in vitro*. Br J Pharmacol 103:1733–1739. CrossRef Medline

Ishikawa T, Kaneko M, Shin HS, Takahashi T (2005) Presynaptic N-type and P/Q-type Ca^{2+} channels mediating synaptic transmission at the calyx of held of mice. J Physiol 568:199–209. CrossRef Medline

Iwasaki S, Takahashi T (2001) Developmental regulation of transmitter release at the calyx of held in rat auditory brainstem. J Physiol 534:861–871. CrossRef Medline

Kawaguchi Y, Kubota Y (1997) GABAergic cell subtypes and their synaptic connections in rat frontal cortex. Cereb Cortex 7:476–486. CrossRef Medline

Kisvárday ZF, Beaulieu C, Eysel UT (1993) Network of GABAergic large basket cells in cat visual cortex (area 18): implication for lateral disinhibition. J Comp Neurol 327:398–415. CrossRef Medline

Kobayashi M, Inoue T, Matsuo R, Masuda Y, Hidaka O, Kang Y, Morimoto T (1997) Role of calcium conductances on spike afterpotentials in rat trigeminal motoneurons. J Neurophysiol 77:3273–3283. CrossRef Medline

Koester HJ, Johnston D (2005) Target cell-dependent normalization of transmitter release at neocortical synapses. Science 308:863–866. CrossRef Medline

Koyanagi Y, Oi Y, Yamamoto K, Koshikawa N, Kobayashi M (2014) Fast-spiking cell to pyramidal cell connections are the most sensitive to propofol-induced facilitation of GABAergic currents in rat insular cortex. Anesthesiology 121:68–78. CrossRef Medline

Koyanagi Y, Yamamoto K, Oi Y, Koshikawa N, Kobayashi M (2010) Presynaptic interneuron subtype- and age-dependent modulation of GABAergic synaptic transmission by β-adrenoceptors in rat insular cortex. J Neurophysiol 103:2876–2888. CrossRef Medline

Kröner S, Krimer LS, Lewis DA, Barrionuevo G (2007) Dopamine increases inhibition in the monkey dorsolateral prefrontal cortex through cell type-specific modulation of interneurons. Cereb Cortex 17:1020–1032. Medline

Letzkus JJ, Wolff SB, LüthiA (2015) Disinhibition, a circuit mechanism for associative learning and memory. Neuron 88:264–276. CrossRef Medline

Lu JT, Li CY, Zhao JP, Poo MM, Zhang XH (2007) Spike-timing-dependent plasticity of neocortical excitatory synapses on inhibitory interneurons depends on target cell type. J Neurosci 27:9711–9720. CrossRef Medline

Marrion NV, Tavalin SJ (1998) Selective activation of Ca^{2+}-activated K^+ channels by co-localized Ca^{2+} channels in hippocampal neurons. Nature 395:900–905. CrossRef Medline

Mochida S, Few AP, Scheuer T, Catterall WA (2008) Regulation of presynaptic Ca(V)2.1 channels by Ca^{2+} sensor proteins mediates short-term synaptic plasticity. Neuron 57:210–216. CrossRef Medline

Mori M, Tanifuji S, Mochida S (2014) Kinetic organization of Ca^{2+} signals that regulate synaptic release efficacy in sympathetic neurons. Mol Pharmacol 86:297–305. CrossRef Medline

Nagai T, Ibata K, Park ES, Kubota M, Mikoshiba K, Miyawaki A (2002) A variant of yellow fluorescent protein with fast and efficient maturation for cell-biological applications. Nat Biotechnol 20:87–90. CrossRef Medline

Nanou E, Scheuer T, Catterall WA (2016) Calcium sensor regulation of the $Ca_V2.1$ Ca^{2+} channel contributes to long-term potentiation and spatial learning. Proc Natl Acad Sci U S A 113:13209–13214. CrossRef Medline

Neher E, Sakaba T (2008) Multiple roles of calcium ions in the regulation of neurotransmitter release. Neuron 59:861–872. CrossRef Medline

Oleskevich S, Clements J, Walmsley B (2000) Release probability modulates short-term plasticity at a rat giant terminal. J Physiol 524:513–523. CrossRef Medline

Overstreet LS, Jones MV, Westbrook GL (2000) Slow desensitization regulates the availability of synaptic $GABA_A$ receptors. J Neurosci 20:7914–7921. CrossRef Medline

Pattillo JM, Yazejian B, DiGregorio DA, Vergara JL, Grinnell AD, Meriney SD (2001) Contribution of presynaptic calcium-activated potassium currents to transmitter release regulation in cultured Xenopus nerve-muscle synapses. Neuroscience 102:229–240. CrossRef Medline

Pfeffer CK, Xue M, He M, Huang ZJ, Scanziani M (2013) Inhibition of inhibition in visual cortex: the logic of connections between molecularly distinct interneurons. Nat Neurosci 16:1068–1076. CrossRef Medline

Porter JT, Johnson CK, Agmon A (2001) Diverse types of interneurons generate thalamus-evoked feedforward inhibition in the mouse barrel cortex. J Neurosci 21:2699–2710. CrossRef Medline

Raffaelli G, Saviane C, Mohajerani MH, Pedarzani P, Cherubini E (2004) BK potassium channels control transmitter release at CA3-CA3 synapses in the rat hippocampus. J Physiol 557:147–157. CrossRef Medline

Reyes A, Lujan R, Rozov A, Burnashev N, Somogyi P, Sakmann B (1998) Target-cell-specific facilitation and depression in neocortical circuits. Nat Neurosci 1:279–285. CrossRef Medline

Rozov A, Burnashev N, Sakmann B, Neher E (2001) Transmitter release modulation by intracellular Ca^{2+} buffers in facilitating and depressing nerve terminals of pyramidal cells in layer 2/3 of the rat neocortex indicates a target cell-specific difference in presynaptic calcium dynamics. J Physiol 531:807–826. CrossRef Medline

Satake S, Imoto K (2014) Cav2.1 channels control multivesicular release by relying on their distance from exocytotic Ca^{2+} sensors at rat cerebellar granule cells. J Neurosci 34:1462–1474. CrossRef Medline

Scheuber A, Miles R, Poncer JC (2004) Presynaptic Cav2.1 and Cav2.2 differentially influence release dynamics at hippocampal excitatory synapses. J Neurosci 24:10402–10409. CrossRef Medline

Schneggenburger R, Neher E (2005) Presynaptic calcium and control of vesicle fusion. Curr Opin Neurobiol 15:266–274. CrossRef Medline

Silver RA (2003) Estimation of nonuniform quantal parameters with multiple-probability fluctuation analysis: theory, application and limitations. J Neurosci Methods 130:127–141. CrossRef Medline

Silver RA, Momiyama A, Cull-Candy SG (1998) Locus of frequency-dependent depression identified with multiple-probability fluctuation analysis at rat climbing fibre-Purkinje cell synapses. J Physiol 510:881–902. CrossRef Medline

Su SC, Seo J, Pan JQ, Samuels BA, Rudenko A, Ericsson M, Neve RL, Yue DT, Tsai LH (2012) Regulation of N-type voltage-gated calcium channels and presynaptic function by cyclin-dependent kinase 5. Neuron 75:675–687. CrossRef Medline

Takahashi T, Momiyama A (1993) Different types of calcium channels mediate central synaptic transmission. Nature 366:156–158. CrossRef Medline

Takei H, Yamamoto K, Bae YC, Shirakawa T, Kobayashi M (2017) Histamine H_3 heteroreceptors suppress glutamatergic and GABAergic synaptic transmission in the rat insular cortex. Front Neural Circuits 11:85. CrossRef Medline

Toledo-Rodriguez M, Blumenfeld B, Wu C, Luo J, Attali B, Goodman P, Markram H (2004) Correlation maps allow neuronal electrical properties to be predicted from single-cell gene expression profiles in rat neocortex. Cereb Cortex 14:1310–1327. CrossRef Medline

Tremblay R, Lee S, Rudy B (2016) GABAergic interneurons in the neocortex: from cellular properties to circuits. Neuron 91:260–292. CrossRef Medline

Uematsu M, Hirai Y, Karube F, Ebihara S, Kato M, Abe K, Obata K, Yoshida S, Hirabayashi M, Yanagawa Y, Kawaguchi Y (2008) Quantitative chemical composition of cortical GABAergic neurons revealed in transgenic venus-expressing rats. Cereb Cortex 18:315–330. CrossRef Medline

Wikström MA, El Manira A (1998) Calcium influx through N- and P/Q-type channels activate apamin-sensitive calcium-dependent potassium channels generating the late afterhyperpolarization in lamprey spinal neurons. Eur J Neurosci 10:1528–1532. CrossRef Medline

Xu-Friedman MA, Regehr WG (2004) Structural contributions to short-term synaptic plasticity. Physiol Rev 84:69–85. CrossRef Medline

Yamamoto K, Koyanagi Y, Koshikawa N, Kobayashi M (2010a) Postsynaptic cell type-dependent cholinergic regulation of GABAergic synaptic transmission in rat insular cortex. J Neurophysiol 104:1933–1945. CrossRef Medline

Yamamoto K, Noguchi J, Yamada C, Watabe AM, Kato F (2010b) Distinct target cell-dependent forms of short-term plasticity of the central visceral afferent synapses of the rat. BMC Neurosci 11:134. Medline

Yan Z, Chi P, Bibb JA, Ryan TA, Greengard P (2002) Roscovitine: a novel regulator of P/Q-type calcium channels and transmitter release in central neurons. J Physiol 540:761–770. CrossRef Medline

Yang H, Xu-Friedman MA (2008) Relative roles of different mechanisms of depression at the mouse endbulb of held. J Neurophysiol 99:2510–2521. CrossRef Medline

Zaitsev AV, Povysheva NV, Lewis DA, Krimer LS (2007) P/Q-type, but not N-type, calcium channels mediate GABA release from fast-spiking interneurons to pyramidal cells in rat prefrontal cortex. J Neurophysiol 97:3567–3573. CrossRef Medline

Zucker RS, Regehr WG (2002) Short-term synaptic plasticity. Annu Rev Physiol 64:355–405. CrossRef Medline